Cellular/Molecular

Coronin1A Regulates the Trafficking of Alpha Synuclein in Microglia

Karl E. Biggs,[1,2] Emma N. Fikse,[1] Faith L. Anderson,[1] Arminja N. Kettenbach,[2,3] and Matthew C. Havrda[1,3]
Departments of [1]Molecular and Systems Biology and, [2]Biochemistry and Cell Biology, Geisel School of Medicine at Dartmouth, Hanover, New Hampshire 03766, [3]Dartmouth Cancer Center, Geisel School of Medicine at Dartmouth, Lebanon, New Hampshire 03766

Microglia respond to cytotoxic protein aggregates associated with the progression of neurodegenerative disease. Pathological protein aggregates activate the microglial NLRP3 inflammasome resulting in proinflammatory signaling, secretion, and potentially pyroptotic cell death. We characterized mixed sex primary mouse microglia exposed to microbial stressors and alpha synuclein preformed fibrils (αsyn PFFs) to identify cellular mechanisms related to Parkinson's disease. Microglia package and release the endosome fate regulator Coronin1A (Coro1A) in EVs in an *Nlrp3*-dependent manner in widely used experimental activation conditions. We were surprised to find that Coro1A packaging and release was not *Nlrp3*-dependent in αsyn PFF exposure conditions. *Coro1A*$^{-/-}$ microglia exposed to αsyn PFFs trafficked more αsyn to the lysosomal compartment increasing lysosomal membrane permeabilization. This corresponds to a decrease in αsyn released in EVs suggesting that Coro1A functions to shunt pathological proteins to a secretory pathway to attenuate lysosomal stress. αsyn PFF-driven lysosomal stress resulting from *Coro1a* loss was associated with enhanced cytotoxicity. Intrinsic apoptosis signaling was unaffected, but we observed elevated cytosolic cathepsin B and the presence of a cathepsin-associated 55 kD PARP cleavage product. Postmortem analysis of the PD mesencephalon supported a role for Coro1A in microglia, revealing elevated levels of Coro1A protein in human PD brains compared with those of healthy donors. Findings are relevant to the distribution of pathological αsyn and indicate that *Coro1a* protects microglia from lysosomal overload, inflammasome activation, and pyroptotic demise.

Key words: **alpha synuclein; extracellular vesicle; lysosome; microglia; NLRP3; Parkinson's disease**

Significance Statement

Microglia are responsible for clearing toxic protein aggregates such as alpha synuclein (αsyn) in Parkinson's disease (PD). PD is slowly progressive, implying that microglia are under proteinaceous stress for an extended time, maintaining some level of homeostasis while attempting to clear pathologically aggregated proteins. Pathological proteins can overload the lysosomes resulting in rupture, decreasing the ability of microglia to clear protein aggregates, and contributing to a hyperreactive inflammatory state. We determined that the protein Coronin1A functions in microglia to attenuate αsyn-induced lysosomal stress, preventing Nlrp3 inflammasome activation, and cell death. These findings identify a protective cellular mechanism operating in microglia that may contribute to the distribution of pathological proteins into the microenvironment.

Received July 8, 2024; revised Dec. 28, 2024; accepted Jan. 11, 2025.

Author contributions: K.E.B., A.N.K., and M.C.H. designed research; K.E.B., E.N.F., and F.L.A. performed research; K.E.B., A.N.K., and M.C.H. analyzed data; K.E.B. and M.C.H. wrote the paper.

This work was supported by the National Institutes of Health (NIH), National Institute for Environmental Health Sciences [R01 ES033462 and R01ES024745 (M.C.H.)] and grants to A.N.K. from NIH (R35 GM119455). The Life Sciences Light Microscopy Facility at Dartmouth is supported by NIDDK P30/DartCF (P30-DK117469), NCI Cancer Center Support Grant (P30 CA023108), and bioMT COBRE (P20-GM113132). The super-resolution spinning disk confocal (SoRa) is supported through NIH award S10OD032310 to Dr. Yashi Ahmed (PD). Work would not have been possible without infrastructure and technical support available within the Dartmouth Cancer Center (National Cancer Institute (NCI) Cancer Center Support Grant 5P30 CA023108-44). We thank Dr. Chris Shoemaker for his valuable insights on autophagic flux and his generous sharing of key reagents for the autophagic flux experiments; Dr. Ashley Mason for her critical commentary and feedback on the manuscript; Ann Lavanway of the Dartmouth Life Sciences Light Microscopy Facility and Scott Palisoul of the Dartmouth Pathology Shared Resource; Dr. Bruce Stanton, Roxana Barnaby, and Carolyn Winston for their expertise and making available the NanoSight NS300 instrument; Drs. Stephen Lee and Mary Feldman for ongoing support and clinical insights; Drs. William Hickey and Harker Rhodes for their work in establishing and maintaining a biorepository critical for all postmortem tissue analyses at Dartmouth; and Dr. Richard Flavell (Yale School of Medicine) for supplying the *Nlrp3*$^{-/-}$ mice used in the study.

The authors declare no competing financial interests.

F.L.A.'s present address: Merck, Boston, Massachusetts.

Correspondence should be addressed to Matthew C. Havrda at matthew.c.havrda@dartmouth.edu or Arminja N. Kettenbach at arminja.n.kettenbach@darmtouth.edu.

https://doi.org/10.1523/JNEUROSCI.1337-24.2025

Introduction

Microglia play a key role in the progression of neurodegenerative proteinopathies, including Parkinson's disease (PD; Goedert et al., 2017). PD is characterized by the misfolding, aggregation, and accumulation of the small (14 kDa) intrinsically disordered protein alpha synuclein (αsyn). αsyn aggregation manifests in human PD patients as histopathologically detectable Lewy bodies and Lewy neurites in neurons alongside evidence of microglial reactivity and neuroinflammation (Tansey and Romero-Ramos, 2019). Distressed neurons release αsyn, which is phagocytosed by microglia that attempt to clear the pathological aggregates using the endolysosomal machinery (Kim et al., 2013; Choi et al., 2020a,b). αsyn aggregates are resistant to degradation (Tanik et al., 2013) and have been shown to rupture microglial lysosomes resulting in reduced degradative capacity and increased inflammatory state of the microglia (Freeman et al., 2013; Bussi et al., 2018). Sustained stress incurred by αsyn can dysregulate microglia, increasing immunological reactivity that ultimately contributes to neuronal death (Bartels et al., 2020). In an attempt to prevent this hyperreactivity, microglia can transfer αsyn aggregates using direct microglia–microglia contact (Scheiblich et al., 2021b). Furthermore, microglia release αsyn-laden extracellular vesicles (EVs) that can be taken up by neurons propagating the spread of αsyn pathology (Guo et al., 2020) although the reason for this EV release is unknown. Intracellular mechanisms regulating the packaging and release of αsyn-laden EVs by microglia remain poorly characterized and improved understanding of how microglia manage PD-related stress on the endolysosomal system will inform efforts to better detect, monitor, and treat the disease.

Microglial proteinaceous stress also generates danger signals recognized by pattern recognition receptors like the NLRP3 inflammasome. Inflammasome activation is a key aspect of microglial activation associated with a transition to a proinflammatory, secretory phenotype (Anderson et al., 2023). This secretory phenotype includes the release of mature cytokines like IL1B, as well as a poorly defined subset of EVs (Zhang et al., 2017; Budden et al., 2021). NLRP3 inflammasome activation also activates the pore-forming protein gasdermin D (GSDMD) which can lead to an inflammatory, lytic form of cell death called pyroptosis (Liu et al., 2016). NLRP3 activity has now been established as a key mediator of neuroinflammation in PD by our laboratory and others (Gordon et al., 2018; von Herrmann et al., 2018). The intracellular mechanisms regulating early stages of the interaction between the NLRP3 inflammasome and proteinaceous stressors remain poorly defined.

Coro1A encodes Coronin1A, a WD (tryptophan aspartic acid) repeat domain containing protein conserved in vertebrates (Human Gene ID: 11151) that performs various functions related to actin binding, endosome trafficking, and immune function (Pieters et al., 2013). In the nervous system, Coro1A functions in neuronal development and survival signaling in both the peripheral and the central nervous systems (Martorella et al., 2017). Coro1A is widely expressed in hematopoietic cells and has been shown to protect *Mycobacterium tuberculosis* from degradation in bone marrow-derived macrophages (Jayachandran et al., 2007). Coro1A plays a direct role in EV biogenesis in macrophage-like cell lines (Fei et al., 2021), and its expression has been detected postmortem in human microglia (Ahmed et al., 2007). To our knowledge the function of Coro1A in microglia responding to PD-related proteotoxic stress is unknown.

We found that the microglial response to pathological αsyn was distinct from the response to LPS and nigericin. In the context of pathological syn exposure, Coro1A is involved in a mechanism employed in microglia to divert αsyn aggregates toward a secretory pathway. We posit that this buffers the lysosomes to prevent membrane permeabilization (LMP) and Nlrp3-related pyroptosis. Under αsyn-mediated stress, we show that *Coro1a* loss increases the magnitude of lysosomal damage incurred by αsyn PFFs and reduces the release of αsyn in EVs. Our data provides mechanistic insights into the interaction between pathological αsyn, the microglial endolysosomal system, and the NLRP3 inflammasome. These findings inform our understanding of microglial biology under conditions of lysosomal stress and delineate a mechanism relevant to the spread of αsyn pathology.

Materials and Methods

Experimental design

Animals. All mouse experiments were conducted according to the ARRIVE guidelines and approved by the Institutional Animal Care and Use Committee at Dartmouth (Protocol No. 00002117, MCH). Wild-Type (C57BL/J6; RRID: IMSR_JAX:000664) and *Coronin1A*$^{-/-}$ (Strain# 030203; RRID: IMSR_JAX:030203) mice were procured from the Jackson Laboratory and *Nlrp3*$^{-/-}$ mice were generously provided by Dr. Richard Flavell at Yale University under MTA. All animals are on the C57BL/6J genetic background and were housed under standard conditions.

Primary microglia generation. Primary microglia cells were isolated based on the original protocol by Giulian and Baker (1986) and the modified protocol by Scheiblich et al. (2021b). Briefly, brains with the meninges removed from mixed sex, neonatal mice [postnatal days (P) 0–3] were dissociated using 0.25% trypsin without EDTA (Invitrogen, 15050057) and repeated pipetting. Brain homogenate was plated on poly-L-lysine (MilliporeSigma, P4707-50ML) coated T75 culture flasks (2 brains/flask) in DMEM supplemented with 10% heat inactivated fetal bovine serum (FBS) and 1% penicillin/streptomycin (P/S; Invitrogen). On the following day, cells were washed three times with PBS and then cultured in DMEM supplemented with 10% FBS, 1% P/S, and 10% L929 conditioned media as a source of growth factors (Heap et al., 2021). After 7–10 d, loosely attached microglia were shaken off the astrocyte layer by incubation on an orbital shaker for 2 h at 200 rpm. The harvesting procedure was repeated every 2–3 d, for up to 21 d in culture. For experiments, microglia were seeded in appropriately sized well plates allowed to adhere overnight in DMEM/10% FBS/1% P/S and then the following day the cells were washed three times with PBS to remove serum and cultured in serum-free DMEM before experiments were performed. Microglia were isolated from both male and female mice and all cultures are mixed sex.

α-Synuclein PFF generation. Human monomeric alpha synuclein was acquired from Proteos (RP-003) and was validated by Proteos to be endotoxin-free [<0.05 EU/mg via limulus amebocyte lysate (LAL) assay]. To assemble monomeric αsyn into PFFs, we followed the Michael J. Fox Foundation (MJFF) best practices guidelines (Polinski et al., 2018). Briefly, αsyn monomer was centrifuged at 15,000 × *g* and the supernatant was retained, and concentration was measured using a NanoDrop 2000 Spectrophotometer ($\varepsilon = 5{,}960\ M^{-1}cm^{-1}$). The sample was diluted to 5 mg/ml in PBS, pH 7.4 (100 mM NaCl) and placed in a thermomixer to shake at 37°C for 7 d at 1,000 rpm. PFFs were generated by sonicating mature fibrils with 60, 0.5 s pulses at 15% power using a tip sonicator (Branson 250), and the fibrils were allowed to rest on ice every 10 pulses to prevent overheating. Mature fibrils and fragmented PFF generation were confirmed using transmission electron microscopy.

To label αsyn fibrils with ATTO-488 NHS-ester, we followed the method presented in Scheiblich et al. (2021b). Briefly, fibrils were resuspended in two molar equivalents of ATTO-488 NHS-ester (MilliporeSigma, 41698) and incubated for 1 h at room temperature. The reaction was quenched

with 1 mM Tris. The unreacted fluorophore was removed by two centrifugations at 15,000 × *g*.

Cell treatment

All treatments were performed in 6-well cell culture dishes or 24-well culture dishes (only for cell death time course), and cells were plated at a density of 2×10^6 cells/wells (6-well) or 2×10^5 cells/well (24-well). For LPS/nigericin treatments, cells were treated with 10 ng/ml LPS (Sigma Aldrich, L2630) for 24 h and then treated with 10 nM nigericin (Sigma Aldrich, N7143) for 30 min. We acquired human αsyn monomer that is confirmed to be endotoxin-free (<0.05 EU/mg via LAL assay) from Proteos. For αsyn PFF treatment, sonicated PFF concentration was measured (NanoDrop 2000 Spectrophotometer), and PFFs were added to cells at final concentration 2 μM in 2 ml serum-free DMEM. Cells were incubated with PFFs for indicated times. For bafilomycin A treatment, cell were pretreated for 4 h with 1 μM BafA (Cayman Chemical, 11038) before cotreatment with αsyn PFFs. For staurosporine controls, cells were treated with 3 μM staurosporine (Cayman Chemical, 81590) for 4 h. After treatment, conditioned media was collected and cells were harvested with 0.5% trypsin (Life Technologies) and washed with PBS, and the cell pellets and supernatant were saved for further analysis at −80°C.

EV isolation

EVs were isolated using a sequential ultracentrifugation protocol. EV preparations were always done on fresh conditioned media and were never freeze/thawed. Serum-free conditioned media was collected after treatment and immediately centrifuged at 400 × *g* for 4 min at 4°C to pellet cells. The supernatant was transferred to a clean tube and centrifuged at 2,000 × *g* for 10 min at 4°C to pellet dead cells and debris. The supernatant was transferred to clean tubes and centrifuged at 20,000 × *g* for 20 min at 4°C to pellet high density EVs and nonphagocytosed (free) αsyn aggregates. The supernatant was transferred to polycarbonate tubes and subjected to ultracentrifugation at 100,000 × $g_{average}$ (rotor: TH-660; *k*-factor: 44.4; 29,900 rpm) for 120 min at 4°C.

To label EVs with MemGlow 640 dye, we performed the sequential ultracentrifugation protocol until just after the 20,000 × *g* step. The supernatant of the 20,000 × *g* spin was moved to a clean 1.5 ml tube and 5 μl of 20 μM MemGlow 640 stock solution (Cytoskeleton Research, MG04) was added to 1 ml of media for a final concentration of 100 nM MemGlow. The mixture was allowed to incubate for 1 h at RT, followed by centrifugation at 10,000 × *g* for 15 min to pellet unbound dye. The supernatant was then transferred to clean ultracentrifuge tubes and the normal 100,000 × *g* spin was performed to isolate the labeled EVs. Labeled EVs were added to the target WT primary microglia in a 1:1 donor to acceptor ration (i.e., EVs isolated from 2×10^6 cells were split 1:10 to add to 10 chamber slides of cells plated at 2×10^4 cells per chamber slide well).

Nanoparticle tracking analysis

NTA was conducted on a NanoSight NS300. Briefly, immediately following the 100,000 × *g* spin, samples were resuspended in 50 μl of PBS then and diluted 1:100 into 800 μl total volume in PBS. Samples were run on the NanoSight instrument in technical and biological triplicates.

Transmission electron microscopy

For αsyn fibril and PFF morphology, a 10 μl aliquot was adsorbed onto glow discharged 300 mesh carbon/formvar grids (EMS catalog #FCF300-Cu) for 1 min. Samples were fixed with10 μl 2% glutaraldehyde for 1 min then washed three times with diH_2O, and then stained with10 μl of 2% uranyl acetate for 1 min. Images were captured using a Gatan OneView CMOS 4K camera attached to an FEI Tecnai F20 transmission electron microscope operating at 200 kV.

For EV morphology, isolated EVs from the P100 fraction were fixed by incubation with 2% glutaraldehyde in a 1:1 ratio (1% final glutaraldehyde concentration) overnight on a rotator at 4°C. Then, 10 μl of the fixed EV solution was adsorbed onto a nonglow discharged 300 mesh carbon/formvar grid (EMS catalog #FCF300-Cu) for 2 min and then stained with 10 μl of 2% uranyl acetate for 30 s. Images were captured using a Gatan OneView CMOS 4K camera attached to an FEI Tecnai F20 transmission electron microscope operating at 200 kV.

Flow cytometry

Cells were detached with 0.5% trypsin (Life Technologies) for 5 min. They were collected, spun down, and resuspended in FACS buffer (PBS + 2% BSA) and blocked for 30 min in ice. Cells were labeled with anti-mouse CD11B-Alexa Fluor 647 conjugated antibody (Bio-Rad Clone 5C6, MCA711A647; RRID:AB_321292) in FACS buffer for 30 min on ice. After labeling, cells were collected and resuspended in 200 μl of ice-cold FACS solution and measured by flow cytometry using the Miltenyi Biotec 8-Color MACSQuant instrument. Data was analyzed using FlowJo (ver. 10).

Immunoblot

Protein was isolated from conditioned media using methanol-chloroform precipitation. Briefly, 1 volume of methanol and 0.25 volumes of chloroform were added to 500 μl of conditioned media, vortexed for 20 s, and centrifuged at 14,000 rpm for 15 min. The top, aqueous phase was removed, and another volume of methanol was added, vortexed for 20 s, and centrifuged at 14,000 rpm for 15 min. The supernatant was removed leaving a pellet of protein.

Samples were lysed (pellets) or solubilized (precipitated conditioned media) in ice-cold RIPA buffer [50 mM Tris-HCl, 1% Triton X-100, 0.5% sodium deoxycholate, 0.1% sodium dodecyl sulfate (SDS), 150 mM NaCl, pH 8.0] containing 1× halt protease and phosphatase inhibitor (PPI; Thermo Fisher Scientific, 78442). Sample concentration was determined using a BCA assay (Thermo Fisher Scientific, 23225). A 4× NuPAGE LDS Sample Buffer (NP0008) as added in a 1:4 ratio to lysed samples, and all samples except those being used to visualize CD81 were supplemented with 5 mM DTT. Samples were boiled for 10 min before loading equal amounts into gels. The NuPAGE system was used for gel electrophoreses with precast 4–12% Bis-Tris protein gels and MES/SDS running buffer (Thermo Fisher Scientific). Gels were transferred to Immobilon-P PVDF membranes (MilliporeSigma, IPVH00010) for immunoblotting. Membranes were blocked in a solution of 5% skim milk powder dissolved in Tris-buffered saline (TBS) and Tween 20 (TBS-T) before overnight incubation with the following primary antibodies at a dilution of 1:1,000 in blocking buffer. Antibodies used are as follows: NLRP3 (CST 15101S, RRID:AB_2722591), IL-1β (Novus NB600-633, RRID:AB_416684, used at 1:500), Caspase-1 (AdipoGen, Casper-1, RRID:AB_2490248) α-synuclein (Abcam MJFR1, RRID:AB_2537217), CD81 (CST D5O2Q, RRID:AB_2714207), Coronin1A (CST 92904, RRID:AB_2800193), TSG101 (Abcam ab125011, RRID:AB_10974262), Alix (CST E6P9B, RRID:AB_2800192), Cytochrome C (CST D18C7, RRID:AB_2637071), Calreticulin (CST D3E6, RRID:AB_2688013), PARP (CST 9532, RRID:AB_659884), P62 (CST D6M5X, RRID:AB_2798858), LC3A/B (CST D3U4C, RRID:AB_2728823). The following day, anti-species horseradish peroxidase (HRP)-conjugated secondary antibodies (Jackson ImmunoResearch, 115-035-003; RRID:AB_10015289, and111-035-003; RRID:AB_2313567; MilliporeSigma AP180P; RRID:AB_92573) and were incubated with the membrane before developing with SuperSignal West Pico PLUS Chemiluminescent Substrate (Thermo Fisher Scientific, 34580). Blots were imaged using a Bio-Rad ChemiDoc MP.

ELISA

Quantitative measurement of αsyn packaging in EVs was quantified using the LEGEND MAX Human α-Synuclein (Colorimetric) ELISA Kit (BioLegend, 448607). EVs were collected and lysed in RIPA + PPI. Samples were run in two technical duplicates and four biological replicates. Optical density was determined at 450 nm with a microplate reader (Bio-Rad iMark).

Lactate dehydrogenase assay

Lactate dehydrogenase (LDH) was detected using the CyQUANT LDH Cytotoxicity Assay (Thermo Fisher Scientific, C20300). Briefly, conditioned media was collected from cultures treated with αsyn PFFs or staurosporine as a positive control. Conditioned media was centrifuged at 12,000 rpm for 30 min at 4°C to remove cellular debris and frozen

at −80°C until LDH analysis. Media was thawed on ice and 100 µl was added to the wells of a 96-well plate. Then, 100 µl of LDH reaction mixture was added to the media. The assay was incubated for 30 min at room temperature protected from light. The colorimetric change was measured on a plate reader (SpectraMax i3x) at 490 nm, and 680 nm corrected (680–490 nm value) absorbance is used. Plain DMEM subjected to the same freeze thaw cycle was used to calculate background LDH activity. Range was determined using untreated culture media as a low (unruptured) control and apoptosis-inducing staurosporine-treated cell culture media as a high (ruptured) control. Background LDH levels present in the media alone were subtracted from all samples. Cytotoxicity was measured using the following equation: (experimental value − low control) / (high control − low control) × 100.

Immunocytochemistry

Cells were plated at a density of 200,000 cells per well in 4-well chambered cover glass slides (Thermo Fisher Scientific) and were fixed in 10% Tris-Acetate Buffered Formalin (Fisher Scientific, SF99-4; 4% PFA by weight) for 10 min. Cells were permeabilized with PBS containing 0.5% Triton X-100 for 10 min. Cells were blocked in PBS containing 5% bovine serum albumin (BSA) for 30 min. The primary antibodies were diluted 1:200 in blocking buffer and incubated for overnight at 4°C. Primary antibodies used are rat anti-galectin-3 (Santa Cruz Biotechnology, SC-23938, RRID:AB_627658), rabbit anti-LAMP1 (Abcam, ab208493, RRID:AB_2923327), and goat anti-cathepsin B (R&D Systems, AF965, RRID:AB_2086949). After primary antibody incubation cells were washed three times in RT PBS. Secondary antibodies (Thermo Fisher Scientific) were diluted 1:1,000 in blocking buffer and incubated at RT for 1 h. Cells were then washed five times in PBS, stained with 1:10,000 Hoechst 33342 (Molecular Probes, H-3570) for 5 min, and then washed three more times in PBS before storage in PBS at 4°C or imaging.

Confocal microscopy

All fluorescent images were obtained using a Nikon Eclipse Ti-E inverted microscope body coupled to a Yokogawa, two-camera (Prime BSI), CSU-W1 SoRa super resolution spinning disk system with a Nikon LU-N4 laser launch, and ASI Piezo Z Stage. All images were obtained with the microscope operating in SoRa mode and either obtained using a 60× PlanAPO objective lens with a 2.8× magnifier for a total magnification of 168× (galectin-3 puncta experiment, dextran/αsyn colocalization experiment, or LAMP1/CTSB colocalization experiment) or using the 60× PlanAPO objective without the magnifier for a total magnification of 60× (αsyn and EV uptake). All images taken at 168× total magnification were deconvolved using Nikon NIS-Elements software using the 3D Richardson-Lucy algorithm set to auto iterations.

Measurement of αsyn load

WT and *Coro1A*$^{-/-}$ microglia cultures were treated with αsyn-488 PFFs and fixed after 15 min or 8 h. Images were all identically processed. Briefly, *z*-stacks of 3.8 µm total height (0.2 µm *z*-step) were max projected, and ROIs around individual cells were manually drawn based on the bright-field contrast channel and integrated density of αsyn was measured for individual cells using Fiji (ImageJ).

Analysis of galectin-3 puncta formation

Matched WT and *Coro1A*$^{-/-}$ cultures were plated, treated with αsyn PFFs, fixed, and stained in parallel to account for possible batch effect of PFFs and artifacts from the primary culture protocol. Images were identically processed. Briefly, images were max projected in the *z* dimension (0.1 µm *z*-step), and regions of interest containing a single cell were created and isolated all using ImageJ (Fiji). An investigator that was blinded to genotype and treatment ID manually scored cells GAL3 puncta number.

Analysis of αsyn colocalization with dextran labeled lysosomes

We added 100 µg/ml dextran-647 to cells in serum-free media and allowed to incubate for 6 h. The media was removed, cells were washed three times with PBS, and fresh media was added. The cells were allowed to rest for 18 h before treatment. Images were identically processed using ImageJ (Fiji). Briefly, a ROI containing a single cell and single *z*-slice was selected, and the appropriate channels were thresholded using Fiji. Colocalization was measured using the Just Another Colocalization Plugin (JaCoP; Bolte and Cordelières, 2006).

Analysis of cathepsin B/LAMP1 overlap and cathepsin B load

Matched WT and *Coro1A*$^{-/-}$ cultures were plated, treated with αsyn PFFs, fixed, and stained in parallel to account for possible batch effect of PFFs and artifacts from the primary culture protocol. Images were identically processed. For total CTSB load measurements, *z*-stacks of 3.8 µm total height (0.2 µm *z*-step) were max projected, and ROIs around individual cells were manually drawn based on the bright-field contrast channel and integrated density of αsyn was measured for individual cells using Fiji (ImageJ). For CTSB/LAMP1 overlap, an ROI containing a single cell and single *z*-slice was selected, and the appropriate channels were thresholded using Fiji. Colocalization was measured using the JaCoP.

Immunohistochemistry

De-identified postmortem tissues ($n = 12$) were obtained from control donors and patients diagnosed with PD and verified by a board-certified neuropathologist. Tissues were obtained and cataloged by the Department of Pathology at Dartmouth-Hitchcock Medical Center (DHMC). No genetic analysis was conducted using these tissues. De-identified tissue was deemed "not human subject" as approved by the Institutional Review Board at Dartmouth-Hitchcock Medical Center.

Immunostains were performed on 5 µm formalin-fixed paraffin-embedded histologic sections using the automated Leica Bond-Max platform. Primary Coronin1a antibody (Abcam, ab72212, RRID:AB_1268222), Iba-1 antibody (Novus NB100-1028, RRID:AB_3148646), and GFAP [Agilent (Dako) Z0334, RRID:AB_10013382] was detected using a postprimary biotin-free alkaline phosphate polymer and fast red chromogen (Leica Biosystems). Coro1A stained slides were imaged using the PerkinElmer Vectra 3 slide scanner. Briefly, whole slides were scanned using an Olympus 4× UPlanSApo NA 0.16 WD. Tissue areas of interest (PAG, VTA, and SNpC) were then imaged using a 20× UPlanSApo NA 0.75 WD (analysis) and a 40× UPlanSApo NA 0.95 WD (representative). Iba-1 and GFAP stained sections were imaged using an Olympus BX51 microscope. Briefly, tissue areas of interest were imaged using a 20× UPlanFL NA 0.5, and representative images of Iba-1 and GFAP morphology were selected.

All analysis was performed on stitched 20× brain images. Analysis of PAG and VTA sections were performed using QuPath (ver. 0.5.0, RRID:SCR_018257). Briefly, ROIs were drawn around brain regions of interest, and automatic positive cell detection was performed using identical settings for all ROIs. Because pigmented neurons in the SNpC have similar optical properties to the fast red chromogen used to label Coro1A positive cells were manually counted in the SNpC. Briefly, a 250 µm × 250 µm grid was overlayed over the SNpC. Four random boxes of the grid were analyzed for positive and negative cells per brain.

TMT-based quantitative proteomics

EVs were collected and lysed in modified RIPA buffer supplemented with an additional 1% SDS and PPI. Protein concentration was determined using a BCA assay (Thermo Fisher Scientific). Proteins were extracted from bulk EV lysate using single pot, solid-phase-enhanced sample preparation (SP3; Hughes et al., 2019). Briefly, bulk EV lysate was incubated with SpeedBead Magnetic Carboxylate Beads (Cytiva, 65152105050250) in 50% ethanol to induce protein binding at 24°C for 5 min at 1,000 rpm. Beads were washed three times with 80% ethanol followed by two washes with 100% acetonitrile. Beads were resuspended in 30 µl of EPPS with 1:100 trypsin (Promega), and on-bead trypsin digest was performed by incubating the mixture at 37°C at 1,200 rpm, overnight. Individual TMTpro reagent aliquots (0.8 mg; Thermo Fisher Scientific) were resuspended in 85 µl of dry acetonitrile, of which 2 µl of reagent was added to each digested peptide aliquot and vortexed. After incubating for 1 h at room temperature, the reactions were quenched with 3 µl of 5% hydroxylamine/200 mM EPPS solution for 10 min, mixed into one 12-plex, acidified with 20% trifluoroacetic acid (TFA), and desalted using Oasis HLB C18 desalting plate.

The desalted multiplex was dried by vacuum centrifugation and separated using the Pierce high pH reversed-phase peptide fractionation kit (Thermo Fisher Scientific) and resuspended in MS grade water containing 7% methanol and 1.5% formic acid. TMT-labeled peptides were analyzed on an Orbitrap Fusion mass spectrometer (Thermo Fisher Scientific) equipped with an Easy-nLC 1200 (Thermo Fisher Scientific), and raw data was searched and processed as previously described (Smolen et al., 2023). The raw data files were searched using COMET (Eng et al., 2013) with a static mass of 229.162932 Da on peptide N-termini and lysines and 57.02146 Da on cysteines and a variable mass of 15.99491 Da on methionines against the target-decoy version of the mouse proteome sequence database (updated 12/01/2019), maximum of three missed cleavages allowed, precursor ion mass tolerance 1 Da, fragment ion mass tolerance ±8 ppm, and filtered to a <1% FDR at the peptide level. Quantification of LC-MS/MS spectra was performed using in-house developed software. Peptide intensities were adjusted based on total TMT reporter ion intensity in each channel and $\log_2$ transformed. p values were calculated using a two-tailed Student's t test, assuming unequal variance.

Statistical analysis

Statistical analysis was performed using GraphPad Prism 10 (RRID: SCR_002798). Statistical tests were performed using unpaired, two-tailed Student's t test with Welch's correction for two groups or one-way ANOVA with Tukey's multiple-comparisons test for multiple groups. What n is for each experiment is described in the associated figure legend. Numerical p values are provided in the figures themselves. LC-MS analysis was performed using Microsoft excel as described in the "TMT-based quantitative proteomics" section of the method details. Volcano plots, PCA, and hierarchical clustering was performed using Perseus (RRID:SCR_015753). Briefly, proteins that were not significantly differently packaged across any of the four groups were filtered out using multiple t tests. PCA was performed using the Benjamini–Hochberg method and a false discovery rate (FDR) cutoff of 0.05. For hierarchical clustering, filtered proteins were z-scored, and clustering was calculated using Euclidean distance and complete linkage. GO enrichment of hierarchical clustering was performed using WebGestalt (RRID: SCR_006786) using the mouse genome as the reference set and an FDR cutoff of 0.05. GSEA was performed using WebGestalt. Enrichment score was calculated by multiplying the $\log_2$ fold change by the $-\log_{10}$ of the p value.

Data availability

Raw MS data for this study are available at MassIVE (MSV000094046) and PRIDE (accession: PXD049288). All data reported in this paper will be shared by the lead contact upon request (lead contact, Matthew C. Havrda; matthew.c.havrda@dartmouth.edu). This paper does not report original code.

Results

Coronin1A is a component of the microglial extracellular vesicle proteome

We prepared purified microglia cultures based on a modified version of the protocol reported by Giulian and Baker and confirmed primary cultures to be ~95% CD11b positive using flow cytometry (Fig. 1*A*). We activated microglial cultures to trigger the release of EVs using the microbial priming and activating agents lipopolysaccharide (LPS), a component of the bacterial membrane of gram-negative bacteria, and nigericin, an antibiotic potassium ionophore derived from *Streptomyces hygroscopicus*. We confirmed microglial NLRP3 activation by Western blot, detecting elevated NLRP3 protein in the lysate and activated cytokines IL-1β and caspase-1, indicative of NLRP3 inflammasome activation in the conditioned media (Fig. 1*B*, Extended Data Fig. 1-1), as we and others have previously reported (Martinez et al., 2017).

We isolated EVs using a differential ultracentrifugation protocol (Fig. 2*A*) and validated EV purity according to the Minimum Information for Studies of Extracellular Vesicles (MISEV; Welsh et al., 2024). Nanoparticle tracking analysis (NTA) confirmed the expected size distribution and concentration of the EVs (Fig. 2*B*), while transmission electron microscopy (TEM) confirmed the morphology of the EVs (Fig. 2*C*). Western blot analysis confirmed the enrichment of known EV proteins, including the intra-EV protein, ALIX, and membrane-bound EV protein CD81, with low levels of common EV contaminants originating from the endoplasmic reticulum (calreticulin) and mitochondria (cytochrome C; Fig. 2*D*, Extended Data Fig. 1-1).

We compared the size and concentration of EVs isolated from WT and *Nlrp3*$^{-/-}$ microglial cultures treated identically with LPS + nigericin or left untreated. EV size did not change significantly across groups although there is a nonsignificant trend of smaller diameter EVs being released from cells treated with LPS + nigericin compared with controls independent of genotype (Fig. 2*E*). There was no significant difference in the concentration of EVs released across the four groups (Fig. 2*F*).

We assayed the EVs using a quantitative tandem mass tag (TMT) proteomic approach to define the EV proteome associated with microglial activation (Fig. 2*G*). We discovered an array of putative immune signaling competent proteins packaged into microglial EVs, many of which were secreted in an *Nlrp3*-dependent fashion (Fig. 2*H*). Gene set enrichment analysis (GSEA) showed significant enrichment for proteins involved in interferon beta response, integrin mediated signaling, and T-cell activation (Fig. 2*I*). Principal component analysis (PCA) identified that proteins packaged into microglial EVs are dependent both on treatment status (±LPS and nigericin) and genotype (WT/*Nlrp3*$^{-/-}$), and we confirmed that the four populations cluster separately and with their respective biological replicates (Fig. 1*J*). Hierarchical clustering characterized distinct up- and downregulated protein clusters that are dependent upon treatment and genotype. We further characterized these clusters using overrepresentation analysis (ORA) as summarized in Extended Data Figure 2-1 and the raw TMT reporter ion intensities used generate Figure 2 and Extended Data Figure 2-1 are provided in Extended Data Table 2-1. The collective data are consistent with previous reports indicating that microglial EVs perform a signaling role in inflammation (Arvanitaki et al., 2024). This analysis of microglia lacking *Nlrp3* is the first instance of defining the specific *Nlrp3*-dependent EVome in cells lacking *Nlrp3* and support previous reports that there is a subset of NLRP3 activation-dependent EVs that are involved in cell-to-cell immune signaling (Zhang et al., 2017; Budden et al., 2021).

We examined the dataset to identify proteins that have been previously implicated in endosome trafficking and EV biogenesis. We identified the protein Coronin1A (Coro1A) which was both highly abundant (132/3552 most abundant protein) and significantly dependent on the presence of *Nlrp3* (2.09 times more abundant in WT EVs, $p = 0.038$; Fig. 2*H*). The role of Coro1A in microglial function is unknown but previous studies in other cell types strongly suggest that Coro1A functions in endosome regulation and EV biogenesis (Jayachandran et al., 2007; Suo et al., 2014; Martorella et al., 2017; Fei et al., 2021).

α-Synuclein PFF treatment results in NLRP3-independent packaging of Coro1A into EVs

Our proteomics data supported a role for Coro1A in the biogenesis of EVs. We sought to further characterize Coro1A using microglial stressors related to neurological disorders. We again exposed primary microglia to LPS and nigericin as described above and compared this exposure with the response to αsyn

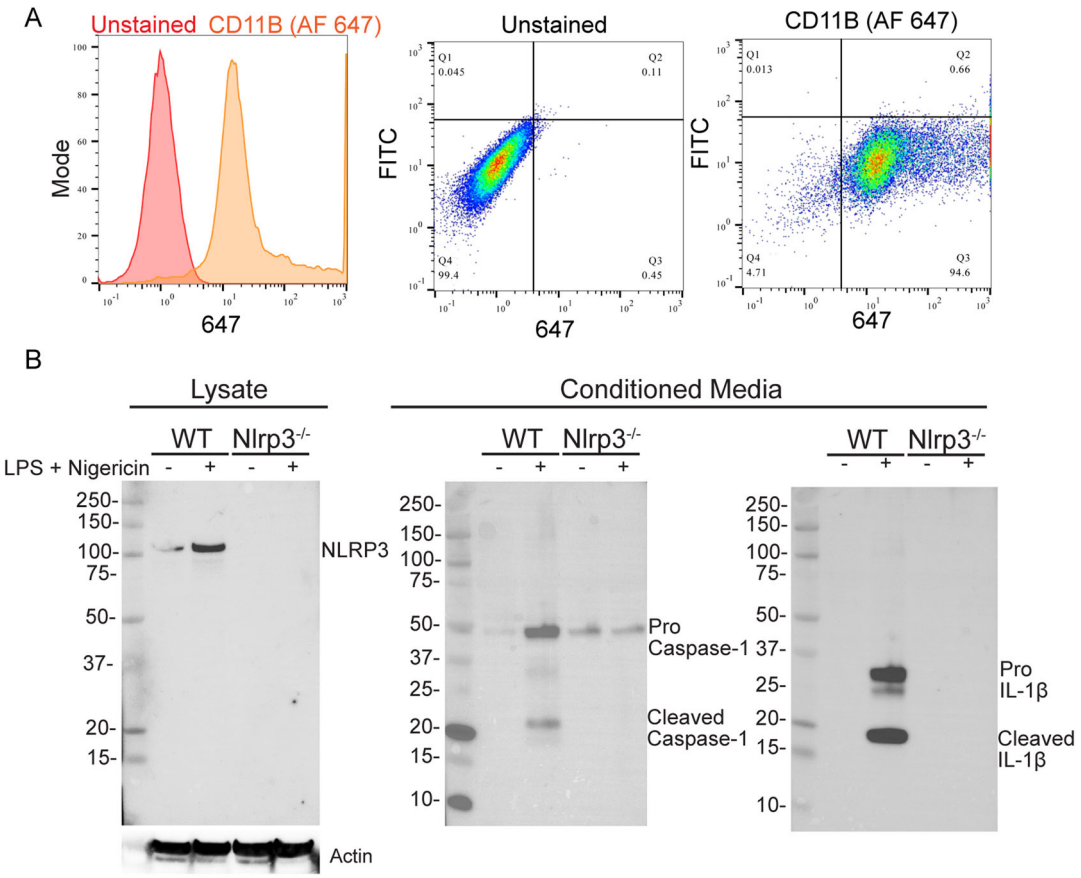

Figure 1. Purification of primary mouse microglia and validation of NLRP3 activation using LPS and nigericin. ***A***, Representative flow cytometry showing purity of primary microglia isolation. Left, Separation between unstained and CD11B stained primary microglia populations. Right, ∼95% of cells are positive for CD11B. ***B***, Representative images of NLRP3-associated proteins (NLRP3, IL-1β, caspase-1) in WT and *Nlrp3*$^{-/-}$ microglia lysates or conditioned media treated with 10 ng/ml LPS for 24 h followed 10 nM nigericin for 30 min. Other two biological replicate Western blots are shown in Extended Data Figure 1-1. Data in ***A*** is representative of three biological replicates run in technical triplicate. Data in ***B*** is representative of biological replicates (shown in Extended Data Fig. 1-1).

PFFs, a PD-relevant proteinopathy model shown to induce endolysosomal stress (Choi et al., 2020b, 2022). We generated and validated αsyn PFFs following the Michael J. Fox Foundation (MJFF) guidelines for PFF generation to maintain consistency with other studies (Polinski et al., 2018; Fig. 3*A*,*B*). We also confirmed that 24 h of treatment with 2 µM αsyn PFFs activates the NLRP3 inflammasome in our WT microglia cultures (Fig. 3*C*, Extended Data Fig. 3-1). We then looked at Coro1A packaging into EVs derived from WT microglia and control cultures established from *Nlrp3*$^{-/-}$ mice either left in a quiescent state, treated with LPS + nigericin, or exposed to 2 µM αsyn PFFs for 24 h. To our surprise, Coro1A packaging into EVs loses its dependency on *Nlrp3* in the αsyn PFF exposure context and is packaged to a similar extent in WT and *Nlrp3*$^{-/-}$ EVs (Fig. 3*D*,*E*). We interpret this to mean that stimulation of the NLRP3 inflammasome in microglia by a PD-related trigger results in a cellular response distinct from that of NLRP3 inflammasome activation resulting from LPS and nigericin. This unexpected finding prompted further characterization of the role of Coro1A in microglia exposed to αsyn PFFs to understand details of this mechanistic divergence relevant to neurodegenerative proteinopathies like PD.

Coro1A loss does not alter the uptake of αsyn PFFs

Coro1A has an established role in endosomal fate in neurons (Suo et al., 2014) and peripheral macrophages (Jayachandran et al., 2007), but the function of Coro1A in microglia remains uncharacterized. We generated primary microglia cultures from WT and *Coro1A*$^{-/-}$ mice and tested whether *Coro1A*$^{-/-}$ microglia phagocytose αsyn PFFs in a manner similar to WT cells. Previous work by another group has shown that primary microglia readily uptake αsyn PFFs within 5 min with robust internalization at 15 min (Scheiblich et al., 2021a). We exposed WT and *Coro1A*$^{-/-}$ primary microglia with 2 µM αsyn PFFs covalently labeled with atto-488 dye (αsyn-488) for 15 min. Using confocal microscopy, we quantified total αsyn fluorescence in over 400 cells per genotype and determined that *Coro1A* loss does not alter αsyn PFF uptake (Fig. 4*A*,*B*). p62-dependent selective autophagy is a proposed mechanism by which microglia clear neuron released αsyn (Choi et al., 2020a,b, 2022). To determine if *Coro1A* loss alters autophagic flux, we exposed WT and *Coro1A*$^{-/-}$ microglia to 2 µM αsyn PFFs for 4 h in the presence or absence of 1 µM bafilomycin A (BafA) to block autophagosome maturation to the lysosome. BafA treatment blocks autophagosome maturation and causes the buildup of LC3 II and p62 proteins and is used as a positive control for complete blockage of autophagic flux (Mauvezin and Neufeld, 2015). We observed no significant changes in p62 and a significant increase of LC3II only when comparing *Coro1A*$^{-/-}$ microglia treated with BafA and no αsyn to *Coro1A*$^{-/-}$ microglia treated with BafA and treated with αsyn. This suggests that αsyn exposure induces autophagy in an additive manner when combined with BafA treatment in *Coro1A*$^{-/-}$ microglia, although the effect is small.

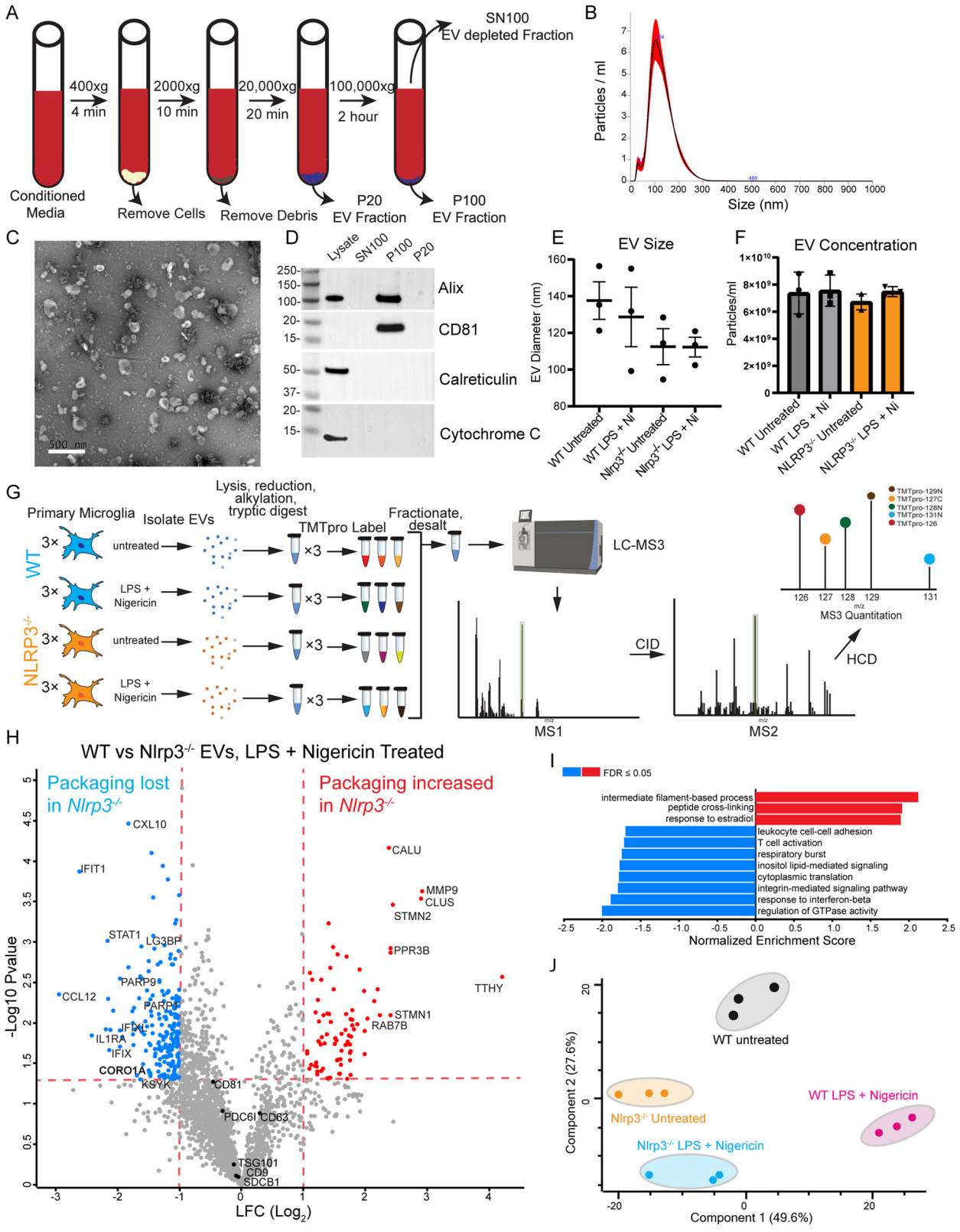

Figure 2. The NLRP3-dependent extracellular vesicle proteome reveals a putative signaling role for microglial EVs and confirms coronin1A as a component of inflammasome EVs. ***A***, Schematic depicting the sequential ultracentrifugation protocol used to isolate EVs. P20 is pellet of 20,000 spin, P100 is pellet of 100,000 spin, SN100 is supernatant from the 100,000 spin. ***B***, Nanoparticle tracking analysis (NTA) of the P100 fraction shows the expected EV size distribution. ***C***, Transmission electron microscopy of P100 EVs showing the expected size and morphology of the EV population. Scale bar, 500 nm. ***D***, Western blot showing enrichment of known EV markers in the P100 EV fraction (Alix, CD81) and minimal contamination from mitochondrial (CytC) and ER (calreticulin) sources as measured by immunoblot. ***E***, NTA analysis of EV size showing no significant difference between groups. ***F***, NTA analysis of EV concentration of EVs released from WT or *Nlrp3*$^{-/-}$ microglia treated with LPS + nigericin showing no significant difference between groups. ***G***, Schematic depicting quantitative proteomics workflow to determine the EVome of microglial EVs from different treatment groups and genotypes. ***H***, Volcano plot of EVs isolated from WT and *Nlrp3*$^{-/-}$ primary microglia treated with LPS and nigericin show a putative NLRP3-dependent signaling role for EVs at the protein level. Proteins in blue are significantly less abundant in *Nlrp3*$^{-/-}$ EVs and are NLRP3-dependent EV components. ***I***, GSEA, biological

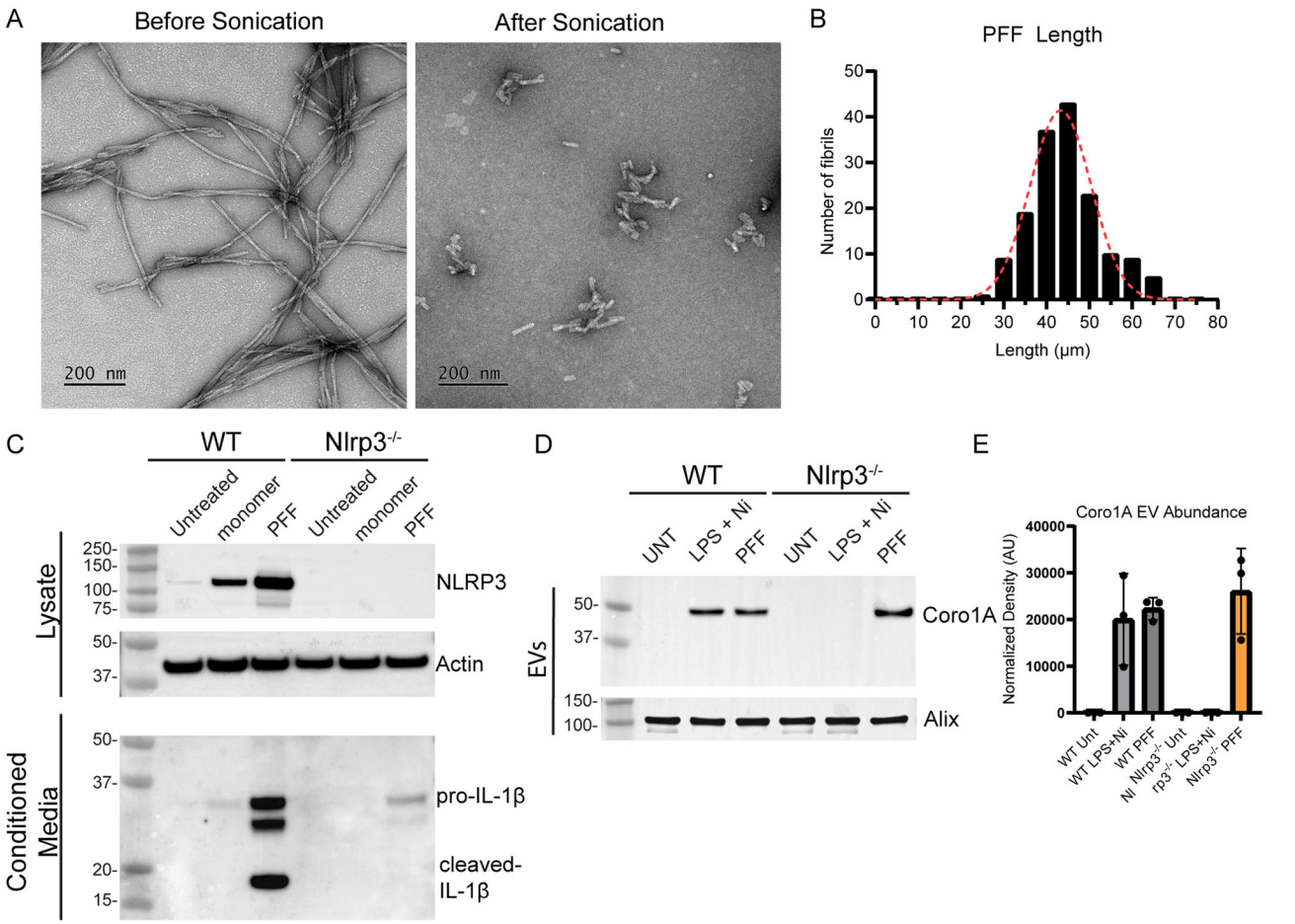

Figure 3. α-Synuclein PFFs but not monomer activate the inflammasome and result in NLRP3-independent packaging of coronin1A into EVs. ***A***, αsyn full length fibrils (left) and sonicated PFFs (right) have the expected morphology observed using TEM. Scale bar, 200 nm. ***B***, The sonicated αsyn PFFs have the correct size distribution according to MJFF guidelines. $n = 157$; average PFF length, 43 μm. ***C***, WT and *Nlrp3*$^{-/-}$ primary microglia were treated with 2 μM αsyn monomer or 2 μM PFFs for 24 h and only PFFs successfully prime and activate the inflammasome in WT cells. Representative images of NLRP3 and IL-1β Western blots in either lysate (NLRP3, actin) or conditioned media (IL-1β) are shown. Biological replicate Western blots are shown in Extended Data Figure 3-1. ***D***, Western blot for Coro1A in EV fraction of WT or *Nlrp3*$^{-/-}$ cells treated with nothing, LPS + nigericin, or αsyn PFFs. ***E***, Quantification of ***D*** showing variance of biological replicates. Data in ***C*** is qualitative and representative of biological triplicate. Images of biological replicates are contained in Extended Data Figure 3-1. Data in ***E*** is mean ± SEM from three biological replicates.

We also observe a trend of lower LC3II levels in BafA-treated *Coro1A*$^{-/-}$ cells not exposed to αsyn compared with identically treated WT cells. This suggests that Coro1A loss may result in a lowered rate of basal autophagy independent of αsyn treatment although this result did not reach statistical significance in this experiment ($p = 0.3387$). This may also be due to microglia lacking *Coro1A*$^{-/-}$ being less sensitive to BafA-mediated blocking of autophagic flux compared with WT microglia. Together our data suggests that *Coro1A* loss does not significantly alter autophagic flux (Fig. 4*C*,*D*). Taken together, these data indicate that Coro1A loss does not alter PFF uptake or autophagic homeostasis under αsyn PFF stress.

More αsyn is trafficked to terminal lysosomal compartments in *Coro1A*$^{-/-}$ microglia

We next examined the lysosomal targeting of αsyn because prior reports indicate that *Coro1A* loss increases the rate of signaling endosome degradation in developing neurons (Suo et al., 2014) and increased *M. tuberculosis* trafficking to lysosomes in peripheral macrophages (Jayachandran et al., 2007). We measured the delivery of αsyn to the lysosome utilizing an antibody-free system based on fluorescently tagged αsyn-488 PFFs coupled with fluorescently labeled dextran-647 to label the terminal lysosomal compartments. Dextran is a readily endocytosed, inert polysaccharide that resists lysosomal degradation. Dextran accumulates in

←

process analysis of differentially packaged EV proteins released from WT and *Nlrp3*$^{-/-}$ microglia treated with LPS and nigericin. ***J***, PCA graph depicting how the EVome depends on both genotype and treatment status. Data in ***B*** is a single biological replicate that is representative of biological triplicate performed in technical triplicate where the red outline the standard deviation of the three technical triplicates. Data in ***D*** is representative of three biological replicates and is qualitative. The variance of biological triplicates is shown in Extended Data Figure 1-1. Data in ***E*** and ***F*** are three biological replicates where each biological replicate is the average of three technical replicates. Statistical analyses were conducted using one-way ANOVA with Tukey's multiple-comparisons test. The *y*-axis in (***H***) is the $-\log_{10}$ of the *p* value as determined by a 2 tailed, unpaired *t* test. The *x*-axis in ***H*** is the $\log_2$ fold change of the TMT channel intensities for each condition. Data in ***I*** was ranked by making a composite score of the $-\log_{10}$ *p* value and the $\log_2$ fold change and analyzed using WebGestalt (Liao et al., 2019). Data in ***J*** was analyzed using Perseus (Tyanova et al., 2016). Extended data table of TMT reporter ion intensities used to generate ***H–J*** is available in Extended Data Table 2-1.

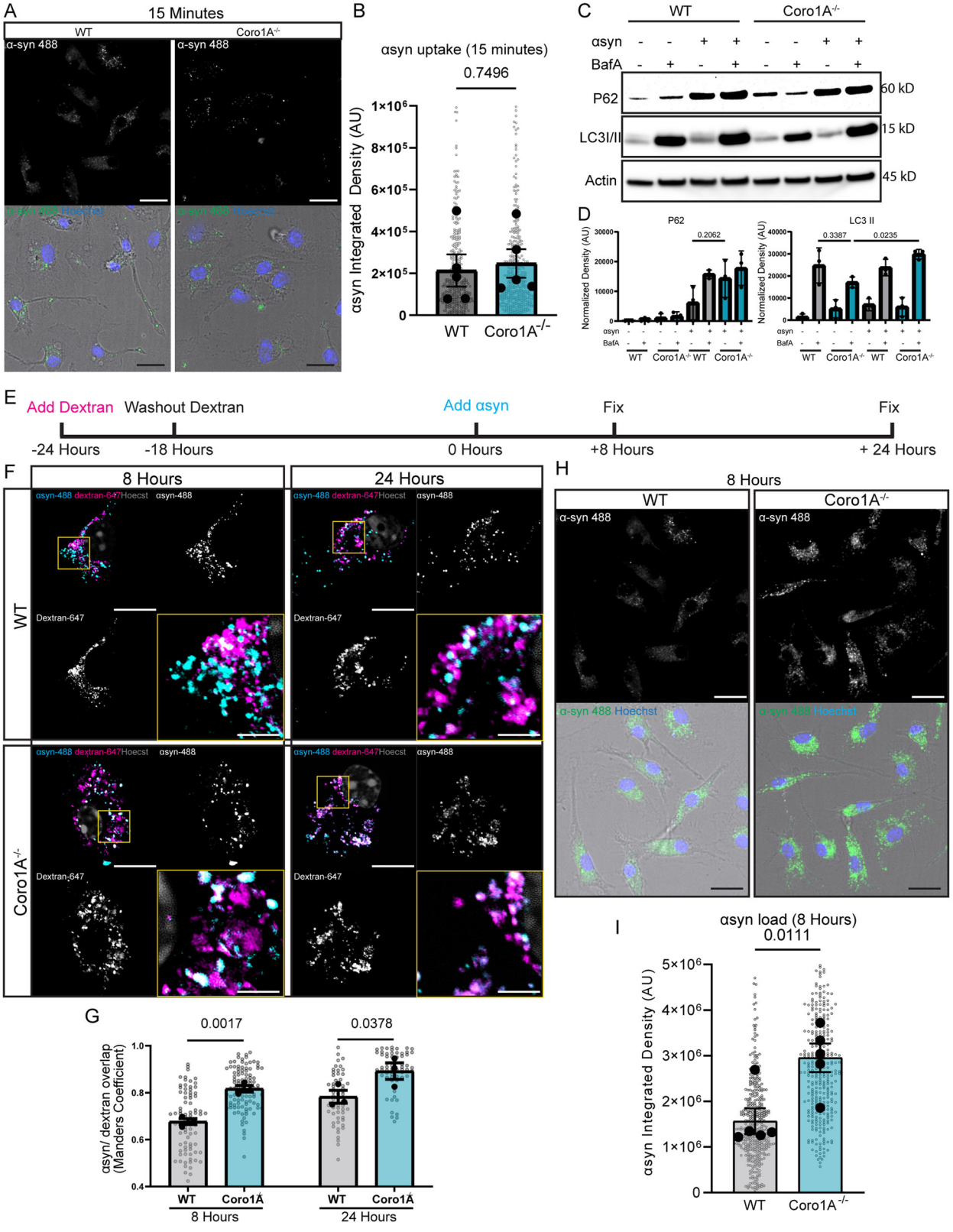

Figure 4. *Coro1a*$^{-/-}$ microglia do not have defects in phagocytosis or autophagy of αsyn PFFs and more αsyn is trafficked to terminal lysosomal compartments in *Coro1A*$^{-/-}$ microglia. ***A***, Representative image of WT and *Coro1A*$^{-/-}$ primary microglia after 15 min of αsyn-488 PFF exposure. Scale bar, 20 µm. ***B***, Quantification of integrated fluorescence intensity in the 488 channel per cell. ***C***, Representative images of the levels of autophagy-related proteins P62 and LC3 I/II and actin loading control in WT and *Coro1A*$^{-/-}$ microglia treated with 2 µM αsyn PFFs for 4 h with and without concurrent treatment with 1 µM bafilomycin A to block autophagosome maturation. ***D***, Quantification of p62 and LC3II shown in ***C***. ***E***, Experimental schematic of dextran-647 labeling paradigm followed by addition of αsyn-488 PFFs. ***F***, Representative single *z*-plane images of WT and *Coro1A*$^{-/-}$ primary microglia exposed to αsyn-488 PFFs for the indicated time points. Terminal lysosomal compartments are labeled with Dextran-647 (magenta), and αsyn-488 is depicted in cyan. Scale bar: top left and gray scale images, 10 µm; zoomed inset (bottom right), 4 µm. ***G***, Measurement of overlap of αsyn with dextran is Mander's coefficient. ***H***, Representative image of WT and *Coro1A*$^{-/-}$ primary microglia after 8 h of αsyn-488 PFF exposure. Scale bar, 20 µm. ***I***, Quantification of integrated fluorescence intensity in the 488 channel per cell. Data in ***B*** mean ± SEM. Five biological replicates with at $n \geq 50$ cells per replicate.

lysosomes, comparing favorably with LAMP1 staining that does not distinguish between late endosomes and lysosomes (Barral et al., 2022; Mulligan and Winckler, 2023). Dextran-647 was incubated with primary microglia for 6 h before being washed off, and the microglia were allowed to rest for 18 h to allow the phagocytosed dextran to build up in terminal lysosomal compartments before treatment with 2 μM αsyn-488 PFFs (Fig. 4*E*). We confirmed that dextran trafficking to the lysosome was similar in WT and *Coro1A*$^{-/-}$ microglia (Extended Data Fig. 4-1). We then evaluated αsyn/dextran colocalization at 8 and 24 h. At both 8 and 24 h, we observed significantly more αsyn colocalized with dextran in *Coro1A*$^{-/-}$ microglia compared with WT microglia (Fig. 4*F*,*G*). Measurement of the amount of αsyn contained within the microglia demonstrated that more αsyn was building up in *Coro1A*$^{-/-}$ microglia compared with WT microglia (Fig. 4*H*,*I*). This implies that αsyn is not being cleared as efficiently in *Coro1A*$^{-/-}$ microglia compared with WT and that this effect is not due to altered phagocytosis or autophagy of αsyn PFFs (Fig. 4*A*–*D*). We then hypothesized that the impaired clearance of αsyn in *Coro1A*$^{-/-}$ microglia may be attributed to increased lysosomal membrane permeabilization (LMP) and concurrent lysosomal dysfunction due to the increased targeting of αsyn to the lysosomes in *Coro1A*$^{-/-}$ microglia.

Coro1A$^{-/-}$ microglia have increased magnitude of lysosomal membrane permeabilization in response to αsyn PFFs

We reasoned that αsyn PFF stress may overload lysosomes causing LMP and lysosomal dysfunction and that this effect may be exacerbated when *Coro1A* is lost (Bourdenx et al., 2014; Dilsizoglu Senol et al., 2021). We measured the kinetics and magnitude of LMP in response to αsyn PFFs using a previously reported and widely used galectin-3 (GAL3)-based fluorescent microscopy assay (Aits et al., 2015). GAL3 is a protein involved in lysosomal repair and lysophagy and is recruited to permeabilized or ruptured lysosomes (Jia et al., 2020). GAL3 recruitment to damaged lysosomes can be visualized as GAL3+ puncta formation on intracellular bodies that are also immunoreactive for the late endosome and lysosome marker LAMP1, hereafter referred to as GAL3+ puncta (Aits et al., 2015). Using this assay, we analyzed WT and *Coro1A*$^{-/-}$ cultures at 0, 4, 8, 12, and 24 h after αsyn PFF treatment. We observed similar levels of basal LMP in both WT and *Coro1A*$^{-/-}$ microglia (Fig. 5*A*–*C*). Figure 5 demonstrates that GAL3+ puncta are more abundant in *Coro1A*$^{-/-}$ cells at earlier time points, indicating αsyn PFF-driven LMP in *Coro1A*$^{-/-}$ microglia occurs both more rapidly and to a greater extent when compared with identically treated WT cells (Fig. 5*A*). After 4 h of αsyn PFF treatment, the number of GAL3+ puncta per cell and the percentage of cells with at least a single GAL3+ puncta were significantly greater in the *Coro1A*$^{-/-}$ microglia (0.9198 vs 5.354 puncta/cell and 31 vs 67% positive cells in WT vs *Coro1A*$^{-/-}$, respectively). This significant trend of increased GAL3+ puncta per cell was maintained across all remaining time points (8 h: 1.361 vs 9.576 puncta/cell; 12 h: 3.582 vs 11.36 puncta per cell; 24 h: 5.453 vs 17.88 puncta per cell; WT vs *Coro1A*$^{-/-}$, respectively; Fig. 5*B*). The percentage of cells with at least one GAL3+ puncta was also significantly greater in *Coro1A*$^{-/-}$ cells at the 8 and 12 h time points compared with WT controls, but the percentage of cells with at least one GAL3+ puncta in WT cultures was similar to the *Coro1A*$^{-/-}$ cultures at 24 h (Fig. 5*C*). The rate of GAL3+ puncta formation in individual cells as well as across the population of cells was calculated by simple linear regression where the slope is taken to be the rate at which these two parameters increase. We found that the amount GAL3+ puncta per cell (i.e., magnitude of lysosomal damage) increased faster in *Coro1A*$^{-/-}$ microglia compared with WT (*Coro1A*$^{-/-}$ slope = 0.6900, $R^2 = 0.8006$; WT slope = 0.2259, $R^2 = 0.4878$; p value = 0.0004). In contrast, we found that the rate of microglia that develop at least one GAL3+ puncta (i.e., microglia whose lysosomes are at least mildly permeabilized) is similar between *Coro1A*$^{-/-}$ and WT cells (*Coro1A*$^{-/-}$ slope = 2.774, $R^2 = 0.6507$; WT slope = 3.006, $R^2 = 0.8796$; p value = 0.7206). Collectively, results thus far support a model in which WT microglia employs a mechanism to counteract αsyn PFF-induced LMP that is independent of NLRP3 inflammasome activity and compromised in the absence of *Coro1A*. This may also result in a vicious cycle where when *Coro1A* is not present, lysosomes are damaged and become less efficient at degrading αsyn which results in increased accumulation of αsyn which causes more dysfunctional lysosomes resulting in a vicious cycle of increasing dysfunction and αsyn accumulation. These results, along with Coro1A's known role in endosome fate determination, suggest that Coro1A mediates a mechanism to alter the fate of αsyn-laden endosomes, and we hypothesized that this alternate fate is an EV secretory pathway.

Coro1A loss severely reduces the amount of αsyn packaged into EVs

Our findings indicate that αsyn fate and subsequent LMP is increased in cells lacking Coro1A. We predict that Coro1A mediates an EV biogenesis pathway to buffer LMP and maintain normal microglial function in response to αsyn aggregates. To test this hypothesis, we assayed αsyn levels in EVs isolated from WT and *Coro1A*$^{-/-}$ EVs to determine if there is less αsyn packaged in EVs released from *Coro1A*$^{-/-}$ microglia. We treated WT and *Coro1A*$^{-/-}$ primary microglia with 2 μM αsyn for 24 h and then isolated EVs via the ultracentrifugation protocol described in Figure 2*A*. Western blot analysis of αsyn in the EV fractions identified significantly more monomeric and high molecular weight (HMW) αsyn species packaged in WT EVs compared with EVs derived from *Coro1A*$^{-/-}$ microglia (Fig. 6*A*). We further controlled for equal loading of EVs using the EV markers described in Figure 2*D*. Levels of the Intra-EV marker Alix are similar in all conditions, but the level of CD81, a membrane-bound EV marker, is significantly increased in WT EVs treated with αsyn but not *Coro1A*$^{-/-}$ EVs treated with αsyn PFFs. This observation has been reported previously in the literature where CD81 was reported to be associated with αsyn-containing EVs released from neurons following inhibition of macroautophagy (Fussi et al., 2018). We further validated that EV levels were consistent across all conditions by immunoblotting against a third EV marker, TSG101 (Fig. 6*C*,*D*). To validate our findings, we

←

Statistical analyses were conducted using two-tailed unpaired *t* test using Welch's correction on the biological replicates ($n = 5$). Data in ***D*** is mean ± SD from three biological replicates. Statistical analyses were conducted using one-way ANOVA with Tukey's multiple-comparisons test. Data in ***G*** is mean ± SEM from three biological replicates with $n \geq 20$ cells per replicate. Small open circles indicate each individual cell measurement and large filled circles represent the mean of each biological replicate. Statistical analyses were performed on the biological replicate values ($n = 3$) and conducted using two-tailed unpaired *t* test with Welch's correction. Data in ***I*** is mean ± SEM from five biological replicates with $n \geq 75$ cells per replicate. Statistical analyses were performed on the biological replicate values ($n = 5$) and conducted using two-tailed unpaired *t* test with Welch's correction.

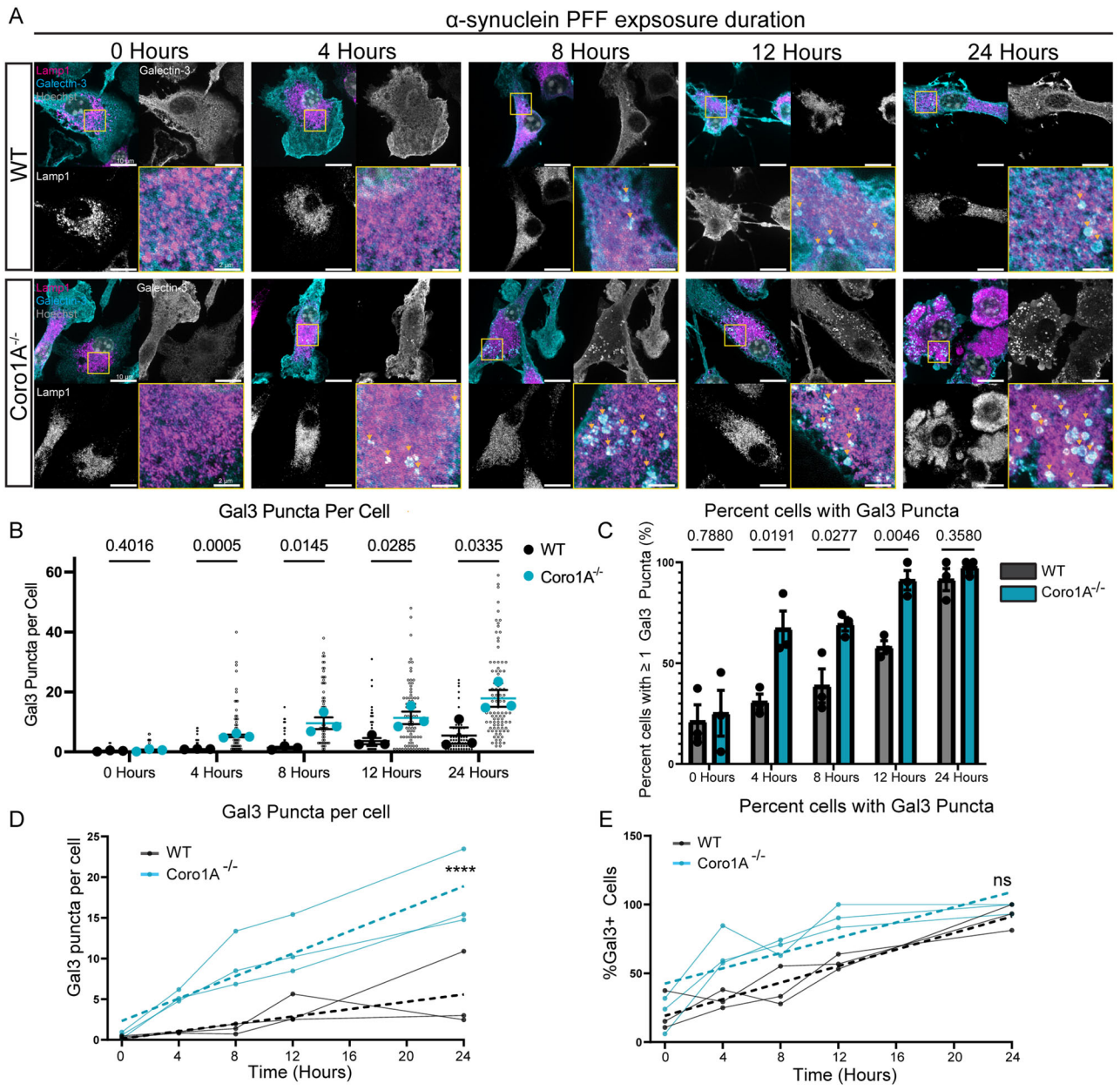

Figure 5. Coro1A knock-out increases the rate and magnitude of lysosomal damage in response to αsyn PFFs. ***A***, Representative maximum projection images of WT and *Coro1A*$^{-/-}$ primary microglia exposed to αsyn PFFs for the indicated times. Late endosomes and lysosomes are labeled with LAMP1 (Magenta). Scale bar: top left and gray scale images, 10 µm; zoomed inset (bottom right), 2 µm. Yellow arrows point to examples of GAL3+ puncta. ***B***, Measurement of GAL3+ puncta per cell. ***C***, Measurement of percentage of cells in each biological replicate that contain GAL3+ puncta. ***D***, The rate (slope) of puncta formation is greater in *Coro1A*$^{-/-}$ cells (*Coro1A*$^{-/-}$ slope = 0.6900, $R^2 = 0.8006$; WT slope = 0.2259, $R^2 = 0.4878$; p value = 0.0004). ***E***, The rate (slope) of having at least one GAL3+ puncta is unchanged in *Coro1A*$^{-/-}$ and WT cells (*Coro1A*$^{-/-}$ slope = 2.774, $R^2 = 0.6507$; WT slope = 3.006, $R^2 = 0.8796$; p value = 0.7206). Data in ***B*** and ***C*** are mean ± SEM from three biological replicates with $n \geq 20$ cells per replicate. In ***B***, small circles indicate each individual cell measurement and large circles represent the mean of each biological replicate. Statistical analyses were performed on the biological replicate values ($n = 3$) and conducted using two-tailed unpaired t test with Welch's correction. Data in ***D*** and ***E*** were calculated using simple linear regression with testing if slopes are significantly different.

used a total αsyn ELISA to quantitatively measure the amount of αsyn packaged in EVs and found that an average of 2.3 µg of αsyn is packaged in EVs derived from WT microglia, whereas only 0.76 µg of αsyn is packaged into EVs derived from *Coro1A*$^{-/-}$ microglia (Fig. 6*E*). Using NTA we measured EV concentration and EV size of the different groups. We found that EV concentration is dependent on αsyn treatment status, not genotype. WT and *Coro1A*$^{-/-}$ microglia release similar concentrations of EVs, and this concentration is significantly increased in both genotypes upon αsyn exposure (Fig. 6*F*). A similar effect is observed when examining EV size where the diameter of WT and *Coro1A*$^{-/-}$ microglia are similar and the diameter of EVs is significantly increased in both genotypes upon αsyn exposure (Fig. 6*G*).

Microglia transfer αsyn from microglia to microglia using EVs and this process is impaired by Coro1A loss

Microglia have been reported to distribute proteinaceous cargo through direct microglia to microglia contact to "share the load" of attempting to degrade αsyn (Scheiblich et al., 2021b).

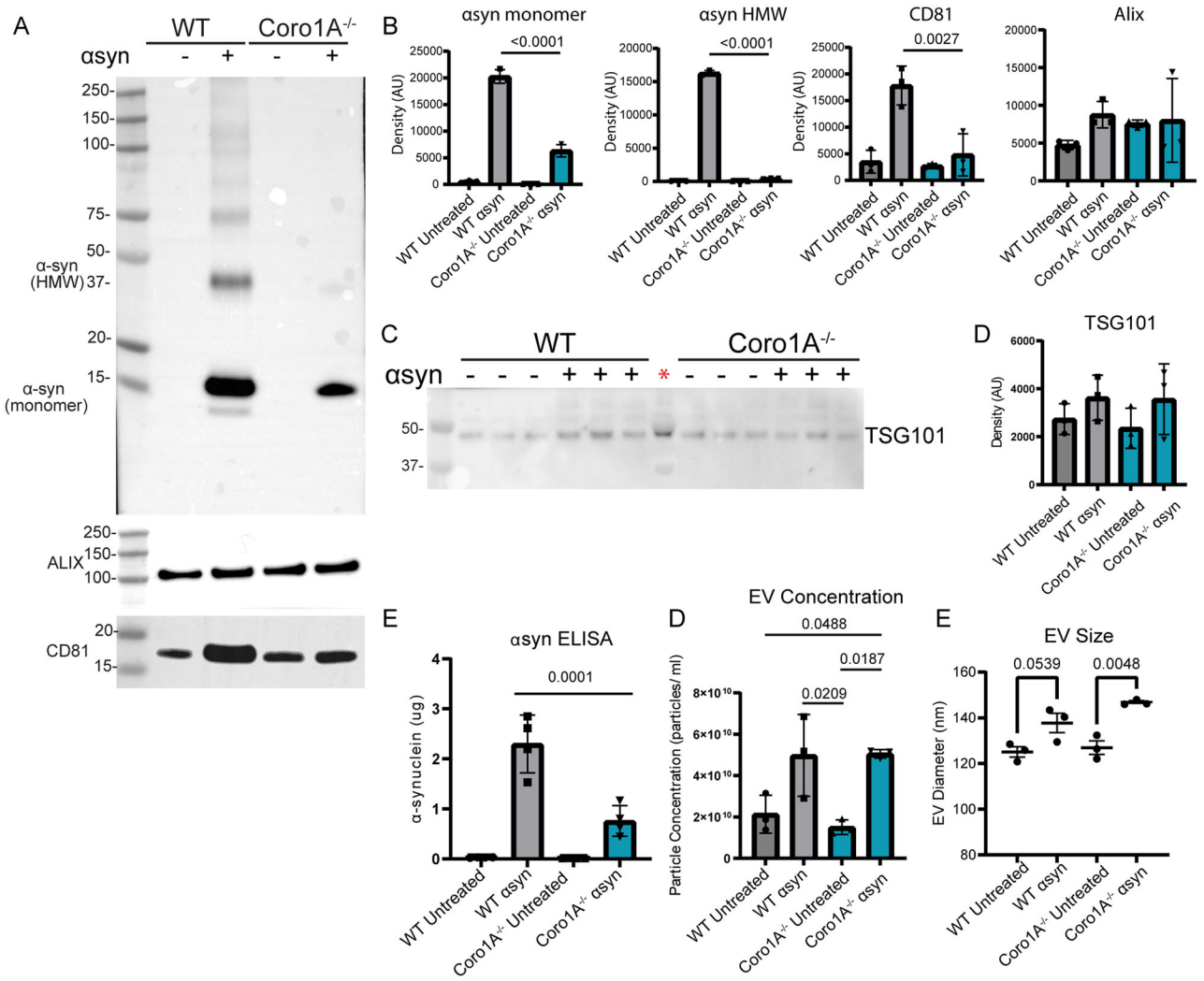

Figure 6. *Coro1A*$^{-/-}$ reduces the amount of αsyn packaged into EVs. ***A***, Representative images of αsyn, or the EV markers ALIX, and CD81 as loading controls in the EV fraction of EVs release from WT or *Coro1A*$^{-/-}$ microglia left in a quiescent state or treated with 2 µM αsyn PFFs for 24 h using immunoblot. ***B***, Quantification of Western blots in ***A***. ***C***, Western blot of the EV marker TSG101 in the EV fraction. Asterisk marks lane that received overflow material from adjacent lanes and is not quantified. ***D***, Quantification of Western blot in ***C***. ***E***, Total human αsyn ELISA of microglial EVs validates that less αsyn is packaged into EVs that are released from *Coro1A*$^{-/-}$ microglia. ***F***, NTA analysis of EV concentration showing that EV concentration is dependent on αsyn treatment status not genotype. ***G***, NTA analysis of EV size in EVs from WT or *Coro1A*$^{-/-}$ microglia treated with LPS + nigericin showing that average EV size is increased in response to αsyn treatment but there is no effect based on genotype. Data in ***B*** and ***D*** are mean ± SD from three biological replicates. Statistical analyses were conducted using one-way ANOVA with Tukey's multiple-comparisons test. Data in ***E*** is mean ± SD from four biological replicates, performed in technical triplicate. Statistical analyses were conducted using one-way ANOVA with Tukey's multiple-comparisons test. Data in ***F*** and ***G*** are biological replicates where each biological replicate value is the average of three technical replicates. Statistical analyses were conducted using one-way ANOVA with Tukey's multiple-comparisons test.

We sought to determine whether αsyn-laden EVs released from microglia could also be trafficked to quiescent microglia to spread the load of toxic αsyn species and if this process was impacted by Coro1A loss. To do this we added αsyn-488 PFFs to WT and *Coro1A*$^{-/-}$ microglia (donor cells), collected EVs after 24 h, and labeled the EVs with a MemGlow 640, a membrane-specific dye that fluoresces in the far-red spectrum. We then added these labeled EVs to quiescent WT microglia (target cells) and allowed the EVs to incubate with the target cells for either 30 min or 20 h, to see if the EVs containing fluorescent αsyn are taken up by quiescent cells (Fig. 7*A*, schematic). We found that significantly more αsyn was taken up by the target cells treated with WT-derived EVs at both the 30 min and 20 h time point (Fig. 7*B*,*C*), consistent with our finding of reduced EV-borne αsyn release by *Coro1A*$^{-/-}$ cultures (Fig. 6*A*–*C*). The amount of total EVs taken up by target cells is dependent on treatment status of the original culture (±αsyn), not genotype (WT/*Coro1A*$^{-/-}$). The total levels of EVs, as measured by MemGlow 640 fluorescence, taken up from αsyn-treated WT and *Coro1A*$^{-/-}$ microglia-derived EVs are similar in magnitude and significantly greater than EVs isolated from untreated WT and *Coro1A*$^{-/-}$ donor cells (Fig. 7*B*,*C*). This data mirrors the EV concentration observations we saw using NTA where the concentration of released EVs is dependent on treatment status and not genotype (Fig. 6*D*).

We also included a no cell control condition where media without cells was treated with 2 µM αsyn-488 PFFs identically to the WT and *Coro1A*$^{-/-}$ cultures and subjected to the same downstream ultracentrifugation and MemGlow labeling, and we observed no fluorescence in either channel (Fig. 7*D*). This ensures that MemGlow does not nonspecifically label free αsyn PFFs (i.e., PFFs that were not taken up by microglia) and that

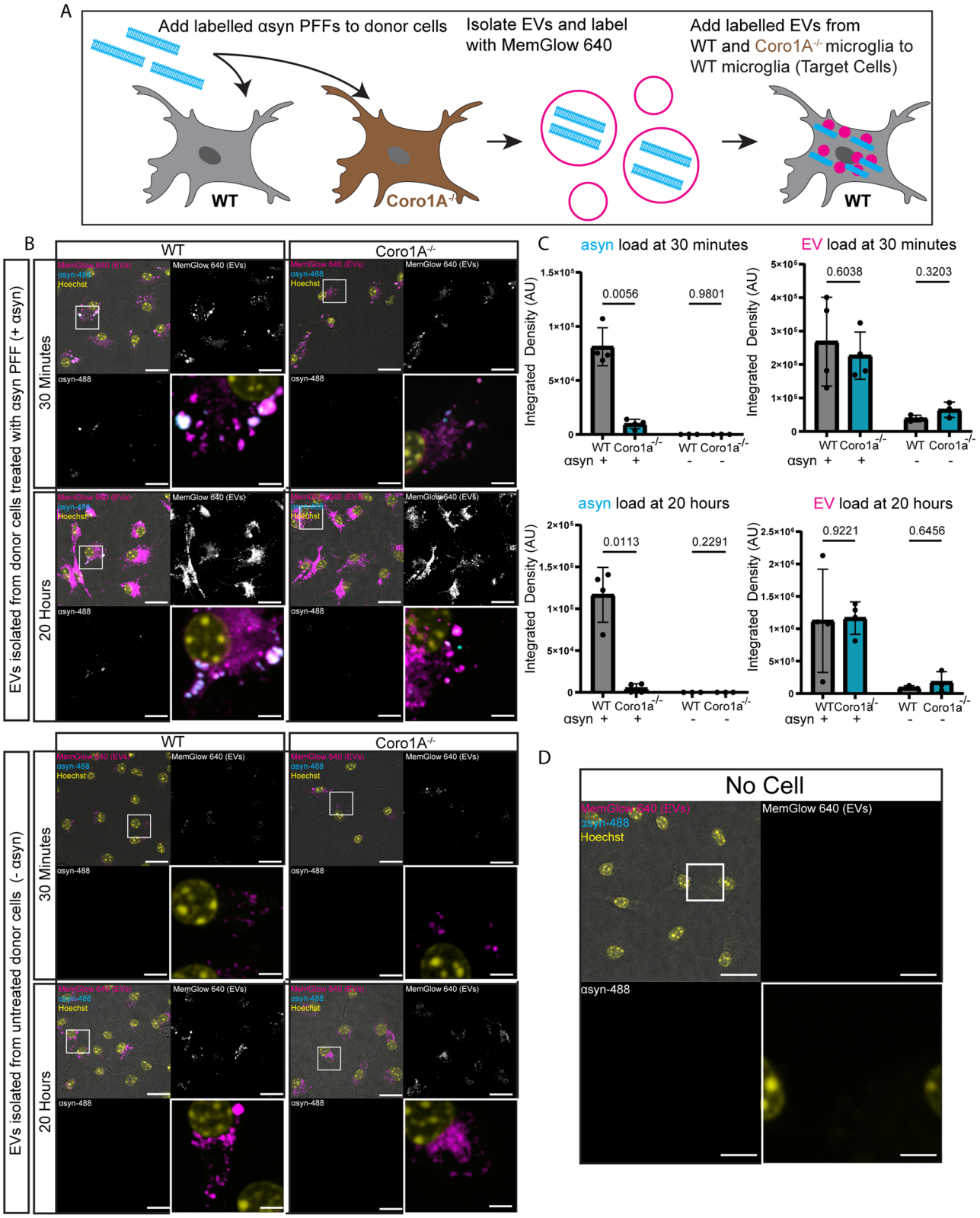

Figure 7. Microglia transfer αsyn from microglia to microglia using EVs and this process is impaired by Coro1A loss. ***A***, Schematic of experimental set up for EV uptake assay. ***B***, Representative images WT microglia treated with different EVs for either 30 min or 20 h. EVs were isolated from WT or *Coro1A*$^{-/-}$ primary microglia treated with αsyn-488 PFFs for 24 h or left untreated for 24 h. Scale bar, 20 µm and 4 µm (bottom right, zoom). ***C***, Quantification of αsyn uptake (cyan) and EV uptake (magenta) at 30 min and 20 h time points. ***D***, No cell control where media was identically treated with 2 µM αsyn-488 PFFs, subjected to the same ultracentrifugation protocol and identically labeled with MemGlow 640. Data in ***C*** is mean ± SEM from three or four biological replicates with $n \geq 20$ cells per replicate. Statistical analyses were conducted using multiple unpaired *t* tests with Welch's correction on the biological replicate values ($n = 3$ or 4).

any free or non-taken up αsyn PFFs are successfully removed by the sequential centrifugation protocol prior to the final 100,000 × *g* spin allowing reliable assessment of only internalized EV-borne αsyn in this experiment.

Coro1A-mediated EV release prevents NLRP3 inflammasome activity protecting microglia from cell death

Neuroprotective pathways are widely studied, but few reports of microglial protective mechanisms in the context of αsyn pathology are available. Therefore, we looked at the consequence of Coro1A loss and the corresponding inability of the *Coro1A*$^{-/-}$ microglia to process αsyn PFFs as they relate to NLRP3-centric and other cell toxicity outcomes. We predicted that if Coro1A was not present to buffer LMP, that would result in increased cytotoxicity and cell death. Inflammasome activation also leads to pyroptotic cell death and inflammatory demise, distinct from immunologically silent intrinsic apoptosis. A total of 2 µM αsyn PFFs can activate the inflammasome after 24 h in WT microglia (Fig. 1), and we tested if there was a difference in NLRP3 activation when *Coro1A* is inactivated. We found that treatment with 2 µM αsyn PFFs for 24 h significantly increased NLRP3 activity in *Coro1A*$^{-/-}$ microglia compared with WT microglia. This included elevated intracellular NLRP3 levels, cleavage, and activation of the pyroptosis indicator protein GSDMD, as well as increased activation and release of mature IL-1β into the conditioned media (Fig. 8*A*,*B*).

To further investigate the mechanisms of cell toxicity in WT and *Coro1A*$^{-/-}$ microglial in response to αsyn PFFs, we collected conditioned media and cell lysate from primary microglia up to 3 d post αsyn PFF addition. We performed Western blot analysis on the lysate and looked for cleaved PARP products to identify if apoptotic or necroptotic cell death pathways may also be involved, in addition to pyroptosis, as measured my GSDMD cleavage (Fig. 8*A*,*B*). We only observed a robust cleaved PARP product at ∼55 kD at 72 h post PFF addition in the *Coro1A*$^{-/-}$ microglia (Fig. 8*C*–*E*). This ∼55 kD is not the canonical 86 kD band that is typically associated with apoptosis (Fig. 8*C*, staurosporine control lane) but the ∼55 kD PARP cleavage fragment has been shown to be produced by cathepsins that may leak from damaged lysosomes (Gobeil et al., 2001; Chaitanya et al., 2010). This finding aligns with our data showing increased LMP in *Coro1A*$^{-/-}$ microglia prompting us to further investigate whether cathepsins are losing their normal colocalization with lysosomal compartments in *Coro1A*$^{-/-}$ exposed to αsyn PFFs.

To do this we exposed WT and *Coro1A*$^{-/-}$ microglia to 2 µM αsyn PFF for 8 or 24 h and then stained the cells with LAMP1 to label late endosomes and lysosomes and cathepsin B (CTSB), a cathepsin implicated in the degradation of αsyn (Sampognaro et al., 2023) and neuroinflammation (Codolo et al., 2013; Branco et al., 2022). We measured both the amount of CTSB in the cell as well as the colocalization of CTSB with LAMP1. We observe that at both 8 and 24 h αsyn treatment durations, there is significantly less CTSB colocalized with late endosome and lysosomal compartments in *Coro1A*$^{-/-}$ microglia (Fig. 8*F*,*G*). This reduction of CTSB/LAMP1 colocalization in *Coro1A*$^{-/-}$ microglia suggests reduced CTSB in late endosome and lysosomal bodies and, coupled with our GAL3 data showing the induction of lysosomal damage responses, suggests CTSB may be leaking out of endosomes/lysosomes and into the cytosol. Our observation of the 55 kD PARP cleavage fragment in Figure 8*C* supports a CTSB leakage model. At basal conditions, we observed much less CTSB overlap with LAMP1 in both WT and *Coro1A*$^{-/-}$ microglia. This may be attributed to less overall CTSB load (Fig. 8*H*), and we also observe a distinct staining pattern of perinuclear CTSB+, LAMP1− areas which suggests that CTSB may still be in the endoplasmic reticulum and not yet transported to endolysosomal compartments as the microglia are in a resting state. We also looked at total CTSB load in the microglia and found that at basal conditions there is significantly less CTSB compared with either of the treatment time points regardless of genotype (Fig. 8*H*). At both the 8 and 24 h time points, total CTSB signal is significantly increased in both genotypes compared with basal conditions (Fig. 8*H*). There is a stepwise increase in CTSB intensity in WT microglia indicating that their degradative capacity is increasing as αsyn load increases. There is no difference in CTSB load between the 8 and 24 h time points in the *Coro1A*$^{-/-}$ microglia. Although not statistically significant, there is a trend of more CTSB signal in the *Coro1A*$^{-/-}$ versus WT microglia at 8 h whereas the inverse relationship is observed at 24 h where the WT microglia have greater CTSB signal than *Coro1A*$^{-/-}$ microglia. This suggests that at earlier time points in the *Coro1A*$^{-/-}$ microglia have a slightly higher degradative capacity but as the *Coro1A*$^{-/-}$ microglia become dysfunctional at longer time points their degradative capacity decreases compared with WT cells which maintain and increase the capacity to degrade αsyn species.

We then sought to determine if cell membrane permeabilization is increased in *Coro1A*$^{-/-}$ microglia in association with increased GSDMD cleavage (Fig. 8*A*), which is indicative of ongoing pyroptosis. We used an LDH assay to determine the level of cell membrane permeability or cytotoxicity at 0, 24, 48, and 72 h time points in WT and *Coro1A*$^{-/-}$ microglia exposed to 2 µM αsyn PFFs. There is no significant increase in cytotoxicity in WT or *Coro1A*$^{-/-}$ microglia at 24 h (Fig. 8*I*). We observe that *Coro1A*$^{-/-}$ microglial cultures are more susceptible to cell membrane permeability as compared with WT microglia at 48 h post PFF addition (Fig. 8*I*). At 72 h, the cytotoxicity levels observed in *Coro1A*$^{-/-}$ microglia decrease compared with those observed in WT microglia. We expect this is due to rupture and cell death occurring between 48 and 72 h in the *Coro1A*$^{-/-}$ microglia which reduces the total amount of *Coro1A*$^{-/-}$ microglia cells in culture and therefore reduces the total pool of LDH available to measure, resulting in decreased LDH levels at 72 h in the *Coro1A*$^{-/-}$ cultures specifically. This is further illustrated by phase contrast images taken of the cultures at 72 h where there is a large amount of cell death observed at 72 h only in *Coro1A*$^{-/-}$ microglia that were also exposed to αsyn PFFs (Fig. 8*K*). We also tested if levels of LDH release in basal conditions are different in WT and *Coro1A*$^{-/-}$ cells to determine if extended time in culture leads to cell death in the absence of αsyn PFFs to ensure we are measuring true cytotoxicity due to only αsyn PFF exposure. We found no difference at any time point tested but did observe that basal LDH release increases at a similar rate for extended times in culture for both WT and *Coro1A*$^{-/-}$ primary microglia (Fig. 8*J*). Taken together, our data suggest inflammasome-mediated pyroptosis as the primary cause of cellular demise in *Coro1A*$^{-/-}$ microglia treated with αsyn PFFs as compared with WT cultures where other nonpyroptotic cell death pathways may contribute.

Coro1A expression is elevated in Parkinson's brain tissues

Reports describe Coro1A function in neuronal development and signaling (Suo et al., 2014). However, another study identified robust expression of Coro1A specifically in microglia, using costaining with known microglia-specific markers and the morphology of the Coro1a stained cells themselves. Furthermore, the

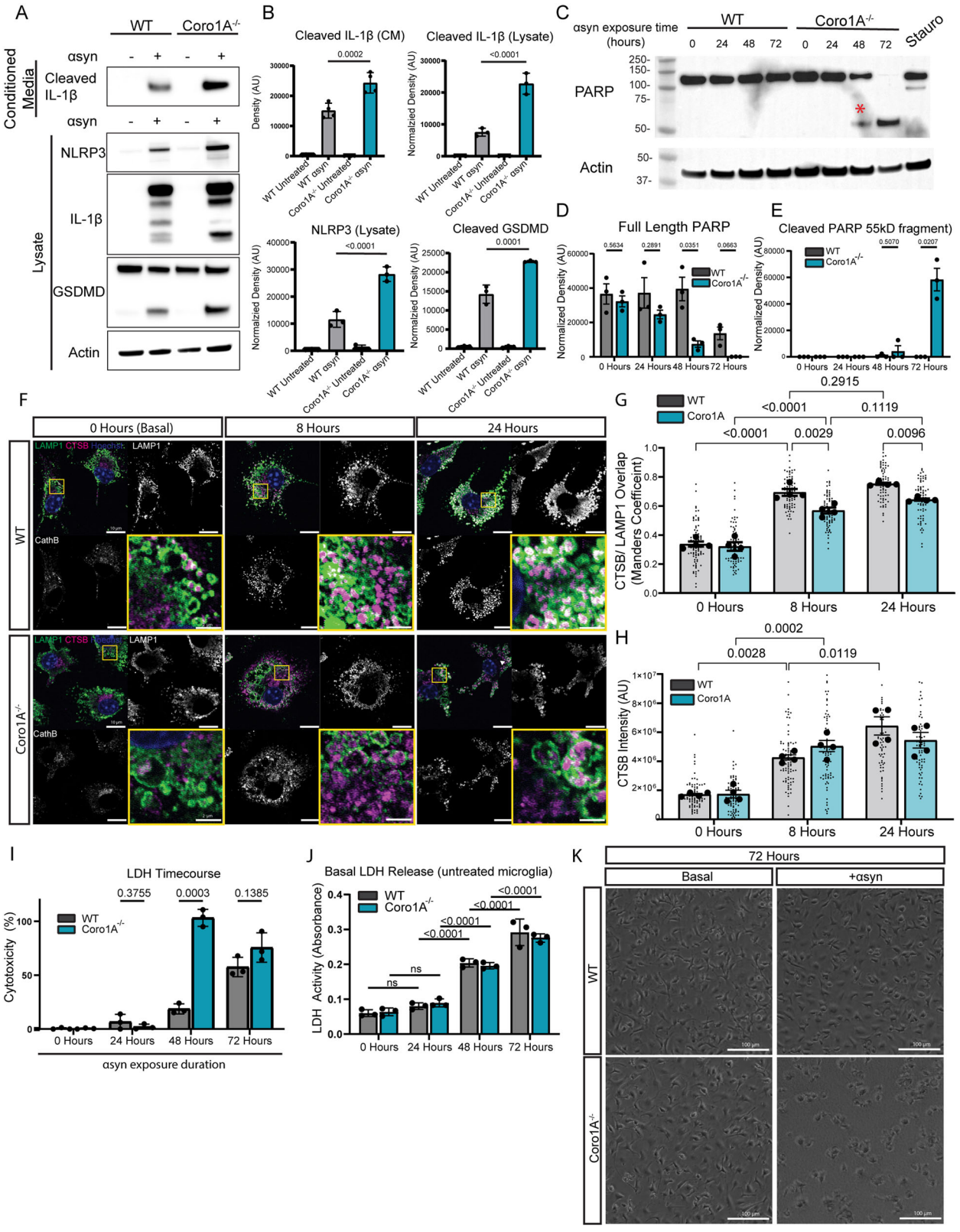

Figure 8. Coro1A-mediated EV release is protective and dampens NLRP3 inflammasome activity and attenuates cell toxicity and death. ***A***, Representative images of NLRP3-associated proteins in the lysate or conditioned media fractions from WT or *Coro1A*$^{-/-}$ primary microglia treated with asyn PFFs or left untreated. ***B***, Quantification of Western blots in ***A***. ***C***, Representative images of cell death marker PARP and actin at indicated time points. Asterisk indicates cleaved PARP band observed only in one biological replicate at 48 h. ***D***, ***E***, Quantification of full length PARP and 55 kD cleaved PARP fragment in ***C***. ***F***, Representative single *z*-plane images of WT and *Coro1A*$^{-/-}$ primary microglia exposed to αsyn PFFs for the indicated time points. Late endosomes and lysosomes are labeled with LAMP1 (green) and cathepsin B is labeled magenta. Scale bar: top left and gray scale images, 10 µm; zoomed inset (bottom right), 2 µm. ***G***, Measurement of overlap of cathepsin B with LAMP1 is measured using Mander's coefficient and was measured in a single *z*-slice. ***H***, Quantification of integrated fluorescence intensity of the cathepsin B signal per cell. ***I***, LDH assay of conditioned media of microglia at indicated time points. Data is normalized to an untreated low control (little/no cell membrane damage) and staurosporine high control (robust cell membrane rupture). ***J***, LDH absorbance (LDH levels) in the conditioned media of WT and *Coro1A*$^{-/-}$ microglia in basal conditions at indicated times. ***K***, Representative phase contrast images of

authors found little or no evidence of Coro1A expression in neurons either in vivo or in vitro and observed similar staining pattern to Iba-1, another widely used marker for microglia in disease (Ahmed et al., 2007). This prompted us to investigate Coro1A expression in the midbrain of human PD patients and healthy controls. We immunolabeled Coro1A in the midbrain of six PD patients and five healthy controls and quantified the percentage of Coro1A positive cells in three regions that have previously been shown to reliably contain robust PD pathology (Seidel et al., 2015). We discovered that in all regions examined (ventral tegmental area, periaqueductal gray, and substantia nigra pars compacta), there are significantly more Coro1A positive cells in PD patients (Fig. 9*A*,*C*). Furthermore, we found that when comparing the brain three brain regions of the PD patients specifically, the SnPC has significantly higher Coro1A immunoreactivity compared with the VTA and PAG. This aligns with the SnPC being the primary location of dopaminergic cell death in PD and where we would expect to see the most proteinaceous and cell death-related damage-associated molecular patterns (DAMPs). We also stained serial sections of the PD brains for Iba-1 to label reactive microglia and GFAP to label astrocytes (Fig. 9*D*) and observe that Coro1A staining closely mimics Iba-1 staining which aligns with the findings by Ahmed et al. that suggests that Coro1A and Iba-1 label similar microglial populations. Taken together we believe Coro1A is staining primarily reactive microglia in these human brain samples although it is possible that low levels of Coro1A are expressed in other cell types such as astrocytes (Pandey et al., 2022) and neurons (Suo et al., 2014; Martorella et al., 2017). Our human data provides evidence that Coro1A-related mechanisms we identified in vitro may be operative in PD.

Discussion

Microglia are a key cell type in the brain responsible for the clearance of toxic protein aggregates associated with the progression of neurodegenerative disease (Li and Haney, 2020). These diseases can progress for decades, so it is important for microglia to maintain cellular processes responsible for protein clearance as long as possible to attempt to combat the accumulation and spread of pathological protein species. Under sustained proteinaceous stress, protein aggregates overload protein clearance pathways, damaging lysosomes and triggering proinflammatory danger sensing signaling modalities. We began our study evaluating widely used inflammasome activators to identify proteins associated with inflammasome-related EV biogenesis. We found that Coro1A was released in EVs in an NLRP3-dependent manner when microglia were stimulated with surrogates for microbial infection. Unexpectedly, proteinaceous insult modeled by αsyn PFF exposure revealed a protective mechanism by which microglial package and shed protein aggregates in EVs. In conditions of *Coro1A* loss, αsyn PFFs accumulate in cells, overwhelm the lysosomes, and trigger inflammasome activation and pyroptotic demise.

We propose a model where Coro1A-mediated αsyn-laden EV release buffers the level of LMP to prevent microglial hyperreactivity, NLRP3 activation, and pyroptotic cellular death (summarized in Fig. 10). There is significant evidence in the literature that cathepsin release from permeabilized lysosomes is a mechanism by which the NLRP3 inflammasome can be activated (Zhou et al., 2016; Chevriaux et al., 2020; Branco et al., 2022). We observed robust LMP and at earlier time points in *Coro1A*$^{-/-}$ compared with WT microglia and the reduction of CTSB colocalization with LAMP1 in *Coro1A*$^{-/-}$ versus WT microglia. This was accompanied by a cathepsin-specific PARP cleavage product observed only in *Coro1A*$^{-/-}$ cells (Gobeil et al., 2001) suggesting that the loss of colocalization we observe between CTSB and LAMP1 in *Coro1A*$^{-/-}$ microglia may be indicative of CTSB release from damaged lysosomes into the cytosol. Furthermore we observe increased cleavage of Caspase-1, IL-1β, and GSDMD and increased cytotoxicity in *Coro1A*$^{-/-}$ microglia compared with WT microglia. We attribute this increase in NLRP3 activation and cell death in *Coro1A*$^{-/-}$ microglia to be primarily attributed to increased lysosomal rupture due to the loss of a *Coro1A*$^{-/-}$-dependent, protective EV biogenesis pathway that shunts toxic αsyn away from the lysosome to a secretory pathway where it can be distributed to other cells. It is possible that *Coro1A*$^{-/-}$ loss affects other pathways that also result in altered immune response and lysosomal homeostasis, but we believe our observed mechanism is one key pathway in modulating cellular response to proteinopathic stress. Determining other pathways that Coro1A loss affects is a promising avenue for follow-up. Coro1A protein expression is increased in human PD brains suggesting that Coro1A plays a role in the etiology of PD. Furthermore, Coro1A has previously been shown to be primarily a microglia-restricted protein in the brain, and our data suggests that this may be the case based on similarity of staining to Iba-1, a widely used reactive microglia marker. More work will be required in human samples to confirm the cell specificity and role of Coro1A in PD etiology.

Our data align with prior work in peripheral macrophages linking Coro1A loss to alterations in endosome fate under *M. tuberculosis* infection (Jayachandran et al., 2007) and another study that identified a role for Coro1A in prolonging signaling endosome survival during neuronal development (Suo et al., 2014). Our data indicate that Coro1A function is also critical for microglial function during disease progression and highlights a mechanism by which reactive microglia may contribute to the spread of αsyn pathology in the interest of their survival. Testing our in vitro model in an in vivo *system* is a particularly promising avenue for follow-up and a priority. This can include both models of PD such as the PFF mouse model (Luk et al., 2012) and in models of general neuroinflammation independent of a specific disease phenotype. It will be particularly informative to measure how readouts of neuroinflammation change but also the effect of Coro1A loss on the ability of αsyn to spread through the brain.

It is still unknown how the Coro1A-mediated EV biogenesis pathway is regulated in the context of αsyn PFF stress. Both Suo et al. and Jayachandran et al. identify calcium signaling as a mechanism to modulate Coro1A function. There has been

←

WT and *Coro1A*$^{-/-}$ microglia left in a quiescent state for 72 h or exposed to αsyn PFFs for 72 h. Data in ***B*** is mean ± SD from three biological replicates. Statistical analyses were conducted using one-way ANOVA with Tukey's multiple-comparisons test. Data in ***D*** and ***E*** are mean ± SD from three biological replicates. Statistical analyses were conducted using multiple unpaired *t* tests with Welch's correction. Data in ***G*** and ***H*** are mean ± SEM from four biological replicates with $n \geq 15$ cells per replicate. Small open circles indicate each individual cell measurement and large filled circles represent the mean of each biological replicate. Statistical analyses were performed on the biological replicate values ($n = 4$) and conducted using one-way ANOVA with Tukey's multiple-comparisons test. Data in ***I*** and ***J*** are mean ± SEM from three biological replicates performed in technical duplicate. Statistical analyses were conducted using two-way ANOVA with Tukey's multiple-comparisons test. Cytotoxicity is defined as: $\text{Cytotoxicity} = \frac{(\text{experimental value} - \text{low control})}{(\text{high control} - \text{low control})} \times 100$.

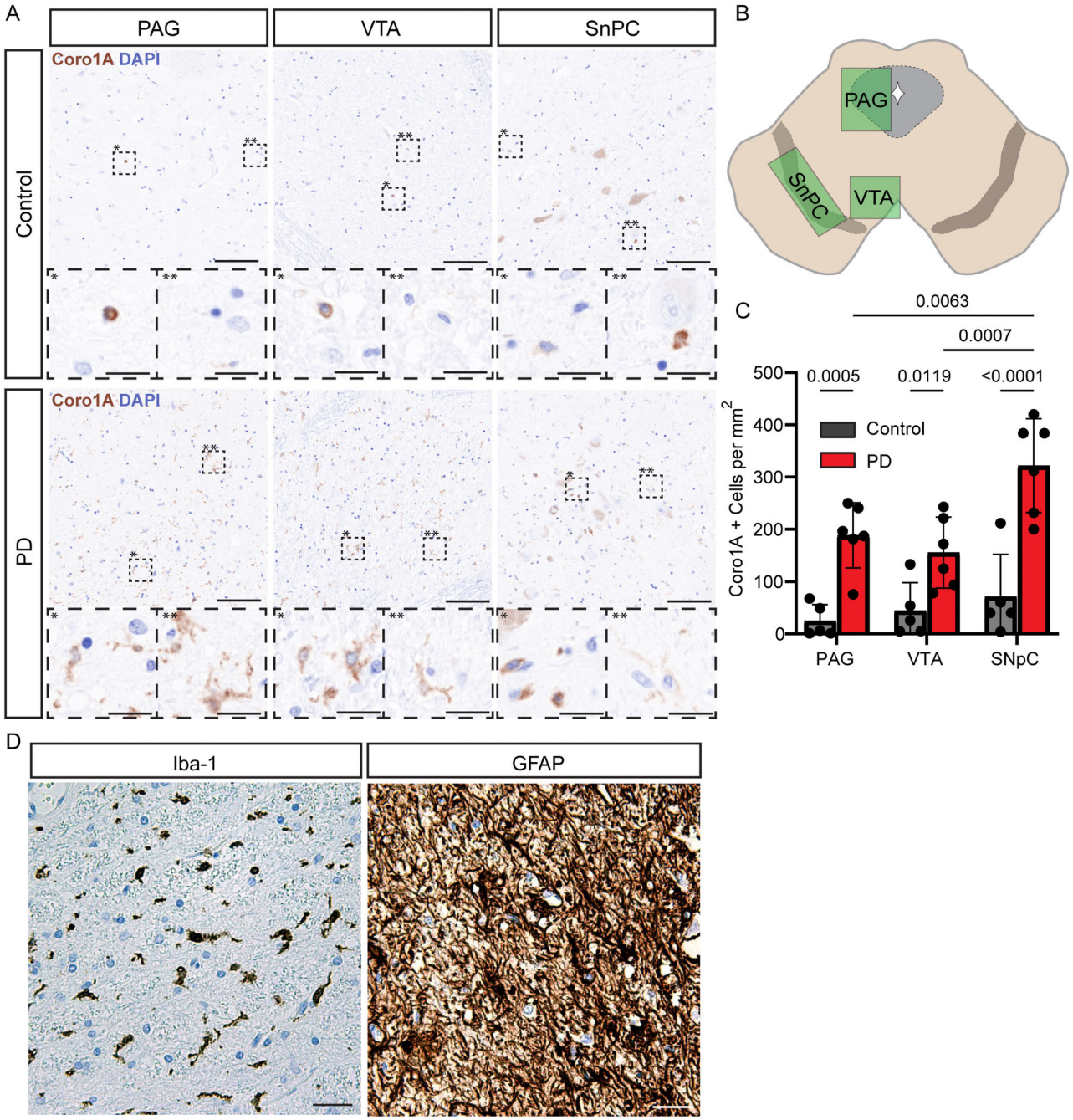

Figure 9. IHC of Coro1A in human control and PD midbrain sections reveals increased Coro1A immunoreactivity in PD patient brains. ***A***, Representative images of Coro1A immunostaining in three different regions of the human midbrain in control and PD patients (PAG, periaqueductal gray area; VTA, ventral tegmental area; SNpC, substantia nigra pars compacta). Scale bar: 100 µm (zoom out) and 20 µm (zoom). ***B***, Representation of where VTA, PAG, and SNpC are located in the human midbrain. ***C***, Quantification of Coro1A positive cells per mm^2 in indicated brain regions. ***D***, Representative image of Iba-1 and GFAP immunostaining in serial PD brain section (scale bar, 20 µm). Data in ***C*** is mean ± SD from five biological replicates for control and six biological replicates for PD. Statistical analyses were conducted using one-way ANOVA with multiple comparisons.

increased interest in lysosomal calcium channels, specifically TRPML1, in neurodegenerative diseases (Scotto Rosato et al., 2019; Tedeschi et al., 2019), and calcium flux through lysosomal channels in response to stress is a possible feedback mechanism by which Coro1A senses and reacts to lysosomal stress.

We show that Coro1A can mediate a shift to favor an EV biogenesis fate over a lysosomal fate. EV release from primary microglia exposed to αsyn PFFs has been previously observed and described to play a role in the cell-to-cell spread of pathology (e.g., microglia to neuron transmission; Guo et al., 2020), but the underlying mechanism of αsyn packaging and subsequent release in microglial EVs was unknown. Our work suggests a Coro1A-mediated mechanism of αsyn packaging into microglial EVs. This model indicates that microglia to neuron transmission observed by Guo et al. (2020) may be the off-target result of microglial EV release and the on-target transfer of αsyn from αsyn impacted microglia to less impacted microglial to clear pathogenic αsyn species. This model is consistent with similar studies implicating microglial tunneling nanotubes as mediators of αsyn distribution among a microglial network (Scheiblich

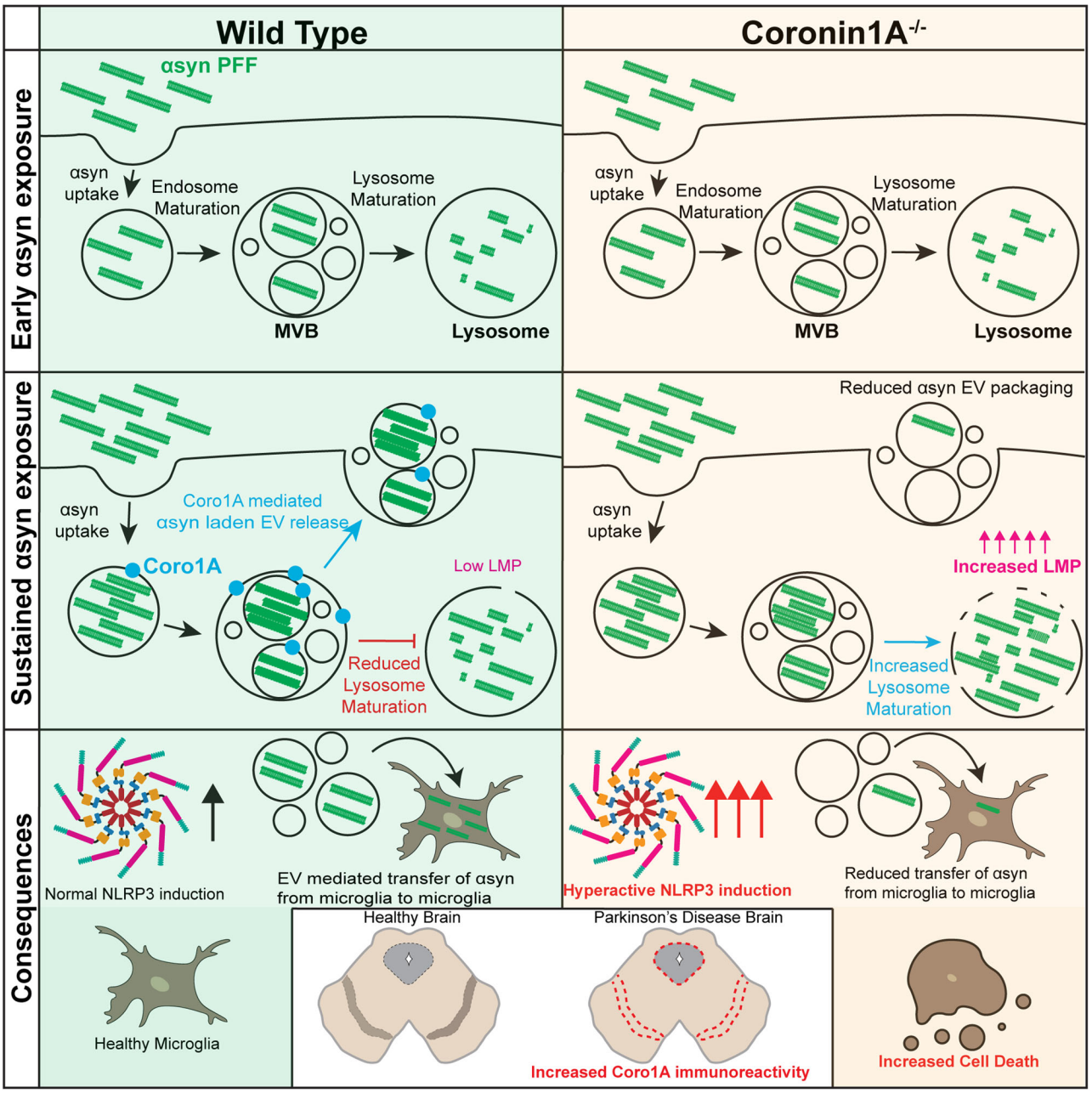

Figure 10. Summary schematic of our proposed mechanism of Coro1A in modulating lysosome health and NLRP3 activity. Summary schematic illustrating our hypothesis that Coro1A functions in microglia to alter the fate of phagocytosed αsyn under sustained proteinopathic stress. Specifically, under sustained αsyn exposure, we propose that Coro1A mediates the release of αsyn-containing endosomes as extracellular vesicles instead of endosomal maturation of αsyn-containing endosomes to the lysosome. Upon loss of Coro1A, this protective mechanism is lost, and lysosomes are overloaded by αsyn aggregates causing lysosomal membrane permeabilization, increased NLRP3 activity, and increased cell death.

et al., 2021b) but invokes αsyn-laden EVs as a potentially more promiscuous mechanism that could result in deleterious microglia to healthy neuron spread. More work is needed to shed light on whether microglia or neurons are more capable of taking up EVs derived from microglia.

The proteomic analysis of EVs released from microglia under LPS and nigericin induced stress implicates Coro1A as an NLRP3-dependent, inflammatory cargo of microglial EVs whereas the NLRP3 dependence is lost under αsyn PFF exposure. Although the field relies on surrogates like LPS and nigericin, it is not surprising that the NLRP3 inflammasome responds differently to sterile triggers such as αsyn PFFs (Couch et al., 2011). This discrepancy may be due to the different mechanism underlying NLRP3 activation in LPS + nigericin versus αsyn contexts. LPS acts on the TLR4 receptor to induce a downstream signaling cascade, which ultimately results in NF-κβ-mediated transcriptional upregulation of proinflammatory proteins such as NLRP3 and IL-1β (Lu et al., 2008), the NLRP3 priming step. Nigericin is a potassium ionophore, and its uptake by primed cells results in a conformational change of NLRP3 itself and, ultimately, activation of the NLRP3 inflammasome (Tapia-Abellán et al., 2021). Like LPS, αsyn PFFs also act on TLR4, although TLR4 seems to predominantly mediate uptake of αsyn, whereas αsyn binding to TLR2 results in upregulation of proinflammatory proteins (Huang et al., 2023). Our findings suggest that lysosomal damage and loss of cathepsin colocalization with

lysosomes is the intracellular trigger for NLRP3 activation in response to αsyn, thus delineating the mechanism of action of αsyn PFF versus LPS + nigericin treatment.

We hypothesize that NLRP3-dependent packaging of Coro1A into EVs in LPS + nigericin treatment mediates the release of NLRP3-related EVs that contain inflammatory signaling proteins as we observe in our mass spectrometry experiment. We further postulate that the incorporation of Coro1A into EVs in the LPS + nigericin paradigm is dependent on NLRP3 activity whether that be priming (LPS) or activation (nigericin) and the incorporation of Coro1A in the αsyn PFF context instead is a response to LMP and NLRP3 agnostic. It is also likely that Coro1A plays additional roles in microglia in neuroinflammation beyond responding to LMP as is evidenced by the dependence on NLRP3 for Coro1A to be packaged into EVs in the LPS + nigericin paradigm, a condition not predicted to result in LMP. It will be important to dissect the role of Coro1A in the *Nlrp3*$^{-/-}$, LPS + nigericin context in similar depth to the αsyn PFF paradigm we describe here as well as exploring neuroinflammatory pathways beyond the NLRP3 inflammasome.

Our findings highlight the pitfalls of modeling NLRP3 activity in proteinopathies such as PD where an LPS priming step is commonly used before treatment of microglia with αsyn PFFs to increase NLRP3 activity (Gordon et al., 2018; Panicker et al., 2019; Scheiblich et al., 2021a). Our findings suggest that LPS pretreatment may confound results relating to αsyn stress and not produce an accurate representation of a disease-relevant cellular response to this stress. Introducing a bacteria-derived stressor such as LPS to cells that reside in the brain is not a physiologic stressor that these cells would be expected to encounter, also possibly contributing to confounding results. We propose Coro1A can play several context-dependent roles that all converge on the packaging and biogenesis of specific populations of EVs in response to different cellular event-related health and disease. The role of Coro1A in the modulation of NLRP3 activity is complex but a promising future direction to investigate given the intense interest in developing NLRP3 inhibitors for clinical use.

References

Ahmed Z, Shaw G, Sharma VP, Yang C, McGowan E, Dickson DW (2007) Actin-binding proteins coronin-1a and IBA-1 are effective microglial markers for immunohistochemistry. J Histochem Cytochem 55:687–700.

Aits S, Jäättelä M, Nylandsted J (2015) Methods for the quantification of lysosomal membrane permeabilization: a hallmark of lysosomal cell death. Methods Cell Biol 126:261–285.

Anderson FL, Biggs KE, Rankin BE, Havrda MC (2023) NLRP3 inflammasome in neurodegenerative disease. Transl Res 252:21–33.

Arvanitaki ES, et al. (2024) Microglia-derived extracellular vesicles trigger age-related neurodegeneration upon DNA damage. Proc Natl Acad Sci U S A 121:e2317402121.

Barral DC, et al. (2022) Current methods to analyze lysosome morphology, positioning, motility and function. Traffic 23:238–269.

Bartels T, Schepper SD, Hong S (2020) Microglia modulate neurodegeneration in Alzheimer's and Parkinson's diseases. Science 370:66–69.

Bolte S, Cordelières FP (2006) A guided tour into subcellular colocalization analysis in light microscopy. J Microsc 224:213–232.

Bourdenx M, Bezard E, Dehay B (2014) Lysosomes and α-synuclein form a dangerous duet leading to neuronal cell death. Front Neuroanat 8:83.

Branco LM, Amaral MP, Boekhoff H, de Lima ABF, Farias IS, Lage SL, Pereira GJS, Franklin BS, Bortoluci KR (2022) Lysosomal cathepsins act in concert with gasdermin-D during NAIP/NLRC4-dependent IL-1β secretion. Cell Death Dis 13:1029.

Budden CF, Gearing LJ, Kaiser R, Standke L, Hertzog PJ, Latz E (2021) Inflammasome-induced extracellular vesicles harbour distinct RNA signatures and alter bystander macrophage responses. J Extracell Vesicles 10:e12127.

Bussi C, et al. (2018) Alpha-synuclein fibrils recruit TBK1 and OPTN to lysosomal damage sites and induce autophagy in microglial cells. J Cell Sci 131:jcs226241.

Chaitanya GV, Alexander JS, Babu PP (2010) PARP-1 cleavage fragments: signatures of cell-death proteases in neurodegeneration. Cell Commun Signal 8:31.

Chevriaux A, Pilot T, Derangère V, Simonin H, Martine P, Chalmin F, Ghiringhelli F, Rébé C (2020) Cathepsin B is required for NLRP3 inflammasome activation in macrophages, through NLRP3 interaction. Front Cell Dev Biol 8:167.

Choi I, Heaton GR, Lee Y-K, Yue Z (2022) Regulation of α-synuclein homeostasis and inflammasome activation by microglial autophagy. Sci Adv 8:eabn1298.

Choi I, Seegobin SP, Liang D, Yue Z (2020a) Synucleinphagy: a microglial "community cleanup program" for neuroprotection. Autophagy 16:1718–1720.

Choi I, Zhang Y, Seegobin SP, Pruvost M, Wang Q, Purtell K, Zhang B, Yue Z (2020b) Microglia clear neuron-released α-synuclein via selective autophagy and prevent neurodegeneration. Nat Commun 11:1386.

Codolo G, Plotegher N, Pozzobon T, Brucale M, Tessari I, Bubacco L, de Bernard M (2013) Triggering of inflammasome by aggregated α-synuclein, an inflammatory response in synucleinopathies. PLoS One 8:e55375.

Couch Y, Alvarez-Erviti L, Sibson NR, Wood MJ, Anthony DC (2011) The acute inflammatory response to intranigral α-synuclein differs significantly from intranigral lipopolysaccharide and is exacerbated by peripheral inflammation. J Neuroinflammation 8:166.

Dilsizoglu Senol A, et al. (2021) α-Synuclein fibrils subvert lysosome structure and function for the propagation of protein misfolding between cells through tunneling nanotubes. PLoS Biol 19:e3001287.

Eng JK, Jahan TA, Hoopmann MR (2013) Comet: an open-source MS/MS sequence database search tool. Proteomics 13:22–24.

Fei X, et al. (2021) Neddylation of Coro1a determines the fate of multivesicular bodies and biogenesis of extracellular vesicles. J Extracell Vesicles 10:e12153.

Freeman D, et al. (2013) Alpha-synuclein induces lysosomal rupture and cathepsin dependent reactive oxygen species following endocytosis. PLoS One 8:e62143.

Fussi N, Höllerhage M, Chakroun T, Nykänen NP, Rösler TW, Koeglsperger T, Wurst W, Behrends C, Höglinger GU (2018) Exosomal secretion of α-synuclein as protective mechanism after upstream blockage of macroautophagy. Cell Death Dis 9:757.

Giulian D, Baker TJ (1986) Characterization of ameboid microglia isolated from developing mammalian brain. J Neurosci 6:2163–2178.

Gobeil S, Boucher CC, Nadeau D, Poirier GG (2001) Characterization of the necrotic cleavage of poly(ADP-ribose) polymerase (PARP-1): implication of lysosomal proteases. Cell Death Differ 8:588–594.

Goedert M, Jakes R, Spillantini MG (2017) The synucleinopathies: twenty years on. J Parkinsons Dis 7:S51–S69.

Gordon R, et al. (2018) Inflammasome inhibition prevents a-synuclein pathology and dopaminergic neurodegeneration in mice. Sci Transl Med 10:eaah4066.

Guo M, Wang J, Zhao Y, Feng Y, Han S, Dong Q, Cui M, Tieu K (2020) Microglial exosomes facilitate α-synuclein transmission in Parkinson's disease. Brain 143:1476–1497.

Heap RE, Marín-Rubio JL, Peltier J, Heunis T, Dannoura A, Moore A, Trost M (2021) Proteomics characterisation of the L929 cell supernatant and its role in BMDM differentiation. Life Sci Alliance 4:e202000957.

Huang Q, Yang P, Liu Y, Ding J, Lu M, Hu G (2023) The interplay between α-synuclein and NLRP3 inflammasome in Parkinson's disease. Biomed Pharmacother 168:115735.

Hughes CS, Moggridge S, Müller T, Sorensen PH, Morin GB, Krijgsveld J (2019) Single-pot, solid-phase-enhanced sample preparation for proteomics experiments. Nat Protoc 14:68–85.

Jayachandran R, Sundaramurthy V, Combaluzier B, Mueller P, Korf H, Huygen K, Miyazaki T, Albrecht I, Massner J, Pieters J (2007) Survival of mycobacteria in macrophages is mediated by coronin 1-dependent activation of calcineurin. Cell 130:37–50.

Jia J, et al. (2020) Galectin-3 coordinates a cellular system for lysosomal repair and removal. Dev Cell 52:69–87.e68.

Kim C, et al. (2013) Neuron-released oligomeric α-synuclein is an endogenous agonist of TLR2 for paracrine activation of microglia. Nat Commun 4:1562.

Li Q, Haney MS (2020) The role of glia in protein aggregation. Neurobiol Dis 143:105015.
Liao Y, Wang J, Jaehnig EJ, Shi Z, Zhang B (2019) WebGestalt 2019: gene set analysis toolkit with revamped UIs and APIs. Nucleic Acids Res 47: W199–W205.
Liu X, Zhang Z, Ruan J, Pan Y, Magupalli VG, Wu H, Lieberman J (2016) Inflammasome-activated gasdermin D causes pyroptosis by forming membrane pores. Nature 535:153–158.
Lu YC, Yeh WC, Ohashi PS (2008) LPS/TLR4 signal transduction pathway. Cytokine 42:145–151.
Luk KC, Kehm V, Carroll J, Zhang B, O'Brien P, Trojanowski JQ, Lee VM-Y (2012) Pathological α-synuclein transmission initiates Parkinson-like neurodegeneration in nontransgenic mice. Science 338:949–953.
Martinez EM, Young AL, Patankar YR, Berwin BL, Wang L, von Herrmann KM, Weier JM, Havrda MC (2017) Editor's highlight: Nlrp3 is required for inflammatory changes and nigral cell loss resulting from chronic intragastric rotenone exposure in mice. Toxicol Sci 159:64–75.
Martorella M, Barford K, Winkler B, Deppmann CD (2017) Emergent role of coronin-1a in neuronal signaling. Vitam Horm 104:113–131.
Mauvezin C, Neufeld TP (2015) Bafilomycin A1 disrupts autophagic flux by inhibiting both V-ATPase-dependent acidification and Ca-P60A/SERCA-dependent autophagosome-lysosome fusion. Autophagy 11: 1437–1438.
Mulligan RJ, Winckler B (2023) Regulation of endosomal trafficking by Rab7 and its effectors in neurons: clues from Charcot-Marie-Tooth 2B disease. Biomolecules 13:1399.
Pandey HS, Kapoor R, Bindu SP (2022) Coronin 1A facilitates calcium mobilization and promotes astrocyte reactivity in HIV-1 neuropathogenesis. FASEB Bioadv 4:254–272.
Panicker N, et al. (2019) Fyn kinase regulates misfolded α-synuclein uptake and NLRP3 inflammasome activation in microglia. J Exp Med 216: 1411–1430.
Pieters J, Müller P, Jayachandran R (2013) On guard: coronin proteins in innate and adaptive immunity. Nat Rev Immunol 13:510–518.
Polinski NK, et al. (2018) Best practices for generating and using alpha-synuclein pre-formed fibrils to model Parkinson's disease in rodents. J Parkinsons Dis 8:303–322.
Sampognaro PJ, Arya S, Knudsen GM, Gunderson EL, Sandoval-Perez A, Hodul M, Bowles K, Craik CS, Jacobson MP, Kao AW (2023) Mutations in α-synuclein, TDP-43 and tau prolong protein half-life through diminished degradation by lysosomal proteases. Mol Neurodegener 18:29.
Scheiblich H, Bousset L, Schwartz S, Griep A, Latz E, Melki R, Heneka MT (2021a) Microglial NLRP3 inflammasome activation upon TLR2 and TLR5 ligation by distinct a-synuclein assemblies. J Immunol 207:2143–2154.
Scheiblich H, et al. (2021b) Microglia jointly degrade fibrillar alpha-synuclein cargo by distribution through tunneling nanotubes. Cell 184:5089–5106.e21.
Scotto Rosato A, et al. (2019) TRPML1 links lysosomal calcium to autophagosome biogenesis through the activation of the CaMKKβ/VPS34 pathway. Nat Commun 10:5630.
Seidel K, et al. (2015) The brainstem pathologies of Parkinson's disease and dementia with Lewy bodies. Brain Pathol 25:121–135.
Smolen KA, Papke CM, Swingle MR, Musiyenko A, Li C, Salter EA, Camp AD, Honkanen RE, Kettenbach AN (2023) Quantitative proteomics and phosphoproteomics of PP2A-PPP2R5D variants reveal deregulation of RPS6 phosphorylation via converging signaling cascades. J Biol Chem 299:105154.
Suo D, Park J, Harrington AW, Zweifel LS, Mihalas S, Deppmann CD (2014) Coronin-1 is a neurotrophin endosomal effector that is required for developmental competition for survival. Nat Neurosci 17:36–45.
Tanik SA, Schultheiss CE, Volpicelli-Daley LA, Brunden KR, Lee VM (2013) Lewy body-like α-synuclein aggregates resist degradation and impair macroautophagy. J Biol Chem 288:15194–15210.
Tansey MG, Romero-Ramos M (2019) Immune system responses in Parkinson's disease: early and dynamic. Eur J Neurosci 49:364–383.
Tapia-Abellán A, Angosto-Bazarra D, Alarcón-Vila C, Baños MC, Hafner-Bratkovič I, Oliva B, Pelegrín P (2021) Sensing low intracellular potassium by NLRP3 results in a stable open structure that promotes inflammasome activation. Sci Adv 7:eabf4468.
Tedeschi V, Petrozziello T, Sisalli MJ, Boscia F, Canzoniero LMT, Secondo A (2019) The activation of mucolipin TRP channel 1 (TRPML1) protects motor neurons from L-BMAA neurotoxicity by promoting autophagic clearance. Sci Rep 9:10743.
Tyanova S, Temu T, Sinitcyn P, Carlson A, Hein MY, Geiger T, Mann M, Cox J (2016) The Perseus computational platform for comprehensive analysis of (prote)omics data. Nat Methods 13:731–740.
von Herrmann KM, Salas LA, Martinez EM, Young AL, Howard JM, Feldman MS, Christensen BC, Wilkins OM, Lee SL, Hickey WF, Havrda MC (2018) NLRP3 expression in mesencephalic neurons and characterization of a rare NLRP3 polymorphism associated with decreased risk of Parkinson's disease. NPJ Parkinsons Dis 4:24.
Welsh JA, et al. (2024) Minimal information for studies of extracellular vesicles (MISEV2023): from basic to advanced approaches. J Extracell Vesicles 13:e12404.
Zhang Y, Liu F, Yuan Y, Jin C, Chang C, Zhu Y, Zhang X, Tian C, He F, Wang J (2017) Inflammasome-derived exosomes activate NF-κB signaling in macrophages. J Proteome Res 16:170–178.
Zhou Y, Lu M, Du R-H, Qiao C, Jiang C-Y, Zhang K-Z, Ding J-H, Hu G (2016) MicroRNA-7 targets Nod-like receptor protein 3 inflammasome to modulate neuroinflammation in the pathogenesis of Parkinson's disease. Mol Neurodegener 11:28.